

A Global Search for Triggered Tremor Following the 2011 M_w 9.0 Tohoku Earthquake

by Kevin Chao,^{*} Zhigang Peng, Hector Gonzalez-Huizar, Chastity Aiken, Bogdan Enescu,[†]
Honn Kao, Aaron A. Velasco, Kazushige Obara, and Takanori Matsuzawa

Abstract The 2011 M_w 9.0 Tohoku, Japan, earthquake triggered deep tectonic tremor and shallow microearthquakes in numerous places worldwide. Here, we conduct a systematic survey of triggered tremor in regions where ambient or triggered tremor has been previously identified. Tremor was triggered in the following regions: south-central Alaska, the Aleutian Arc, Shikoku in southwest Japan, the North Island of New Zealand, southern Oregon, the Parkfield–Cholame section of the San Andreas fault in central California, the San Jacinto fault in southern California, Taiwan, and Vancouver Island. We find no evidence of triggered tremor in the Calaveras fault in northern California. One of the most important factors in controlling the triggering potential is the amplitude of the surface waves. Data examined in this study suggest that the threshold amplitude for triggering tremor is ~ 0.1 cm/s, which is equivalent to a dynamic stress threshold of ~ 10 kilopascals. The incidence angles of the teleseismic surface waves also affect the triggering potentials of Love and Rayleigh waves. The results of this study confirm that both Love and Rayleigh waves contribute to triggering tremor in many regions. In regions where both ambient and triggered tremor are known to occur, tremor triggered by the Tohoku event generally occurred at similar locations with previously identified ambient and/or triggered tremor, further supporting the notion that although the driving forces of triggered and ambient tremor differ, they share similar mechanisms. We find a positive relationship between the amplitudes of the triggering waves and those of the triggered tremor, which is consistent with the prediction of the clock-advance model.

Online Material: Table of measured parameters and other information related to triggering/nontriggering information, and figures of observed seismograms.

Introduction

Following the first discovery of tectonic tremor at the Nankai subduction zone in southwest Japan (Obara, 2002), tremor has been subsequently found along major plate-boundary faults around the Pacific plates (Peng and Gomberg, 2010; Beroza and Ide, 2011, and references therein). Tremor is located mostly below the brittle-ductile transition zone and has extended source duration and nonimpulsive arrivals that lack high-frequency content compared with regular earthquakes in the brittle upper crust. While most tremor occur spontaneously (also known as ambient tremor), sometimes tremor can be instantly triggered by dynamic stresses from regional (Guilhem *et al.*, 2010) or teleseismic earth-

quakes (Miyazawa and Mori, 2006; Rubinstein *et al.*, 2007; Gomberg *et al.*, 2008). Many recent studies suggest that shear faulting is responsible for generating tremor (Shelly *et al.*, 2007; Peng and Gomberg, 2010), and many of the characteristics of triggered and ambient tremor are similar (Shelly *et al.*, 2011). For instance, triggered tremor can mostly be found in regions where ambient tremor is active (Peng and Gomberg, 2010), and their spectral shapes are similar (Rubinstein *et al.*, 2007; Peng *et al.*, 2008). Moreover, at least part of the triggered tremor consists of many low-frequency earthquakes (LFES) that also occur during ambient tremor (Peng *et al.*, 2010; Shelly *et al.*, 2011).

Peng and Gomberg (2010) summarized observations around the world and suggested that teleseismically-induced dynamic stresses on the order of several kilopascals (kPa) are capable of triggering tremor. However, the triggering threshold

^{*}Now at Earthquake Research Institute, University of Tokyo, 1-1-1 Yayoi, Bunkyo-ku, Tokyo 113-0032, Japan.

[†]Now at Earth Evolution Sciences Department, University of Tsukuba, 1-1-1 Tennodai, Tsukuba, Ibaraki 305-8572, Japan.

appears to be variable from region to region. For example, the apparent triggering threshold is about 2–3 kPa at the Parkfield–Cholame section of the San Andreas fault (SAF; Peng *et al.*, 2009), but it is about 8–10 kPa beneath the Central Range in Taiwan (Chao, Peng, Wu, *et al.*, 2012). It is still not clear whether such a difference is caused by different instrumentation or different tremor behavior.

The relationship between surface waves and tremor has been the subject of several recent studies. Gomberg (2010) proposed a clock-advance model in which triggered tremor is considered as sped-up ambient tremor such that the surface-wave stress perturbations exceed the failure threshold of the tremor patch. In particular, the instantaneous perturbed rate is proportional to the background rate, and a function describes how the perturbing stress changes the failure time of a fault patch. Gomberg (2010) further examined the relationship between the amplitudes of the triggering waves and triggered tremor from four observations in Cascadia (Rubinstein *et al.*, 2009) and found that the results did not match the predictions of the clock-advance model. Chao, Peng, Wu, *et al.* (2012) found a positive relationship between the amplitudes of surface waves from nine teleseismic earthquakes and those of triggered tremor beneath the Central Range in Taiwan. In addition, Chao, Peng, Fabian, *et al.* (2012) compared triggered tremor observed in the Parkfield–Cholame section of the SAF with the San Jacinto fault (SJF) in southern California and the Calaveras fault (CF) in northern California. The results suggested that the abundant triggered tremor observations in Parkfield and the relative lack of triggered tremor observations in the other two regions could be related to their background tremor rates. These results suggest a need for further studies that examine the relationship among triggering surface waves, triggered tremor, and background tremor rate.

The 2011 M_w 9.0 Tohoku, Japan, earthquake triggered widespread shallow earthquakes and deep tectonic tremor activity in many places around the world (Miyazawa, 2011; Rubinstein *et al.*, 2011; Wang *et al.*, 2011; Gonzalez-Huizar *et al.*, 2012; Hill *et al.*, 2013; Peng *et al.*, 2013). These observations provide opportunities for testing the clock-advance model (Gomberg, 2010) and understanding the triggering mechanisms and conditions for tremor generation. In this study, we systematically examine triggered tremor during the surface waves of the Tohoku mainshock in many regions where ambient or triggered tremor has been previously observed (Fig. 1 and Table S1 in the electronic supplement). In the following sections, we first show the observations and locations of triggered tremor in each region. Then, we calculate the dynamic stresses of surface waves at various tectonic settings and estimate their triggering potential. Finally, we discuss the prediction of the clock-advance model and the implications of our observations.

Data and Analysis Procedure

The analysis procedure generally follows that of previous studies (Peng *et al.*, 2009; Chao, Peng, Wu, *et al.*, 2012) and

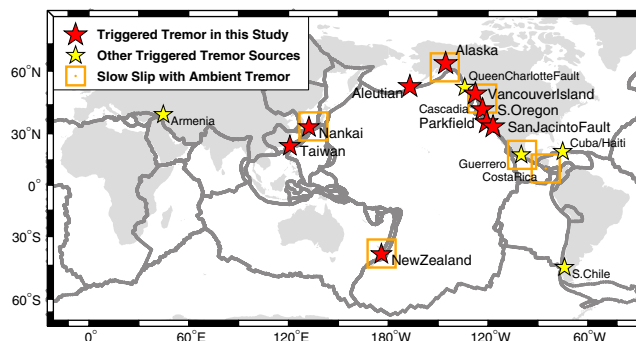


Figure 1. A summary map of triggered and ambient tremor locations around the world. The large stars show the study regions of triggered tremor following the 2011 M_w 9.0 Tohoku, Japan, earthquake. The small stars mark the newly identified regions with triggered tremor reported by recent studies (e.g., Rubinstein *et al.*, 2011; Gonzalez-Huizar *et al.*, 2012; Peng *et al.*, 2012; Zigone *et al.*, 2012; Aiken *et al.*, 2013). Regions where episodic tremor and slow-slip events have been observed are marked as squares. The color version of this figure is available only in the electronic edition.

is briefly described here. We download three-component broadband and short-period seismograms in each region (see Data and Resources), select the data from 1000 s before and 9000 s after the origin time of the Tohoku mainshock, remove the mean of the signals, and generate either band-pass (2–8 Hz) or high-pass (> 5 Hz) filtered seismograms. We also remove the instrument response (i.e., full-frequency response division) to obtain velocity and displacement seismograms and compare them with the high-frequency signals. In each region, we visually inspect the waveforms for potential tremor during the passage of the Tohoku mainshock surface waves, assuming that the tremor signature is a high-frequency non-impulsive signal with no clear P - or S -wave arrivals. We require that the tremor signals be recorded by at least three nearby stations and that the signal-to-noise ratio for tremor is higher than 1.5 (Chao, Peng, Fabian, *et al.*, 2012; Chao, Peng, Wu, *et al.*, 2012). We also compute the spectrogram of seismic data recorded at selected stations (Peng *et al.*, 2011) and use them to help determine the suitable frequency range (2–8 Hz band-pass filter or 5 Hz high-pass filter) and component (i.e., E, N, or Z) that produce the tremor signals.

Once a tremor sequence is identified, we locate each tremor burst by a conventional envelope cross-correlation method (Obara, 2002; Peng and Chao, 2008). Specifically, we search for the location that corresponds to the minimum root mean square (rms) between the theoretical and observed travel-time differences for all possible station pairs. (See Appendix A for detailed analysis procedures.) The error is estimated from the χ -square distribution within a 68% confidence level (Shearer, 1999; Chao, Peng, Wu, *et al.*, 2012). Because the depth is normally not well constrained by using such a method (Chao, Peng, Wu, *et al.*, 2012), we fix the tremor depth to be at 25 km along the SAF and Taiwan, 35 km in the relatively young subduction zones (e.g., southwest Japan, Cascadia), and 45 km in the relatively old subduction zones (e.g.,

the Aleutian Arc, Alaska, and New Zealand). These numbers are primarily based on previous studies, and we also take into consideration the fact that when the age of the subducting plate is older, tremor tends to occur deeper (Ide, 2012).

In regions where tremor appears to come from multiple locations, we divide the seismic data into several groups and locate the tremor of each group separately (see Appendix A). The detailed tremor location information for all regions can be found in Tables 1 and   S1 (available as an electronic supplement to this paper).

Triggered Tremor Observations

In this section, we describe the characteristics of triggered tremor we found in nine of our study regions (Table 1): Nankai, Taiwan, the Aleutian Arc, Alaska, Vancouver Island, southern Oregon, central California, southern California, and New Zealand. In addition, we also include several regions where ambient or triggered tremor have been found in previous studies, but no triggered tremor occurred during the Tohoku mainshock (i.e., the CF in northern California and Guerrero in Mexico) and in regions where the Tohoku mainshock triggered tremor, but were not analyzed in this study (i.e., Cuba; Gonzalez-Huizar *et al.*, 2012; Peng *et al.*, 2013). We sort these regions according to their distances relative to the epicenter of the Tohoku mainshock. We measure the peak ground velocities (PGVs) for the Love and Rayleigh waves shown in the instrument-corrected transverse and vertical-component seismograms, respectively. In addition, we compute the expected PGV at each station based on the surface-wave magnitude M_S equation (Lay and Wallace, 1995; van der Elst and Brodsky, 2010)

$$\log_{10} A_{20} = M_S - 1.66 \log_{10} \Delta - 2, \quad (1)$$

where Δ is the epicentral distance in degrees, and A_{20} is the peak surface-wave displacement at 20 s. We obtain the surface wave magnitude, $M_S = 8.4$, for the Tohoku mainshock based on the empirical estimation (Geller, 1976; Stein and Wysession, 2003). We also assume a predominant period (T) of 20 s for the surface waves and convert the peak displacement (A_{20}) to peak velocity (\dot{u}) with the equation $\dot{u} \approx 2\pi A_{20}/T$ (Aki and Richards, 2002).

Finally, we estimate the corresponding dynamic stress ($\Delta\sigma$) based on equation (2), using a shear rigidity (G) of 35 GPa and a phase velocity (v) of 4.1 and 3.5 km/s for Love (transverse component) and Rayleigh (vertical component) waves, respectively,

$$\Delta\sigma = G\dot{u}/v. \quad (2)$$

Because these are nominal numbers, reasonable changes in their actual values do not substantially change our results. As shown in Figure 2, the epicentral distance mainly controls the PGVs and the associated dynamic stresses for all the regions examined in this study, which is expected from the above two equations. The horizontal dotted line marks the

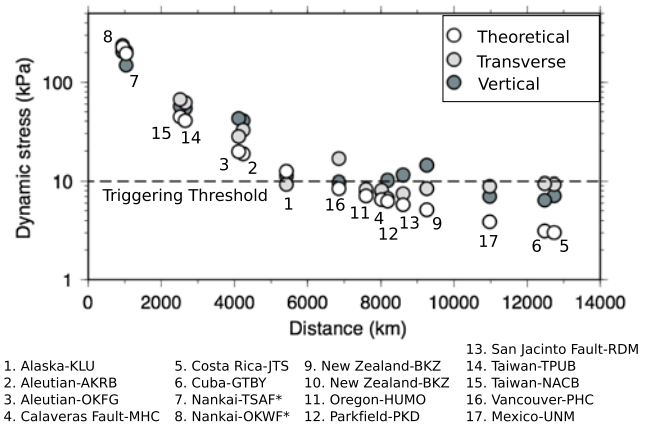


Figure 2. Theoretical and observed dynamic stress in each of our study regions versus epicentral distance to the Tohoku mainshock. Numbers indicate the different study regions and the seismic station used for measuring the peak ground velocity (PGV). The observed dynamic stress is calculated from the PGV of surface waves in transverse and vertical components from the broadband and strong-motion (with * symbol) stations (  Table S2 in the electronic supplement). The horizontal dashed line marks the apparent tremor triggering threshold, which corresponds to a dynamic stress threshold of ~ 10 kPa. The color version of this figure is available only in the electronic edition.

dynamic stress of a triggering threshold of 10 kPa, which corresponds to the measured PGVs of ~ 0.1 cm/s. Note that at distances greater than 9000 km, the observed dynamic stress estimated using equation (2) is approximately 10 kPa and systematically larger than the theoretical values. This is likely caused by the convergence of the surface-wave trains when the great circle distance is larger than 90° .

Nankai, Japan

Widespread ambient tremor activity in the Nankai subduction zone has been the focus of intense study since 2002 (Obara, 2002, 2011; Ide, 2010). While ambient tremor occurs in the Shikoku, Kii, and Tokai regions, parallel to the Nankai trough (Obara *et al.*, 2010), triggered tremor is found in particular spots in these regions (Miyazawa and Mori, 2005, 2006; Miyazawa and Brodsky, 2008). Here we focus only on the Shikoku region because the Kii and Tokai regions are close to the Tohoku epicenter (i.e., less than 800 km) such that early aftershock signals from the Tohoku rupture zone may overprint and obscure any locally triggered tremor signals.

We find at least two tremor sources in Shikoku during the passing surface waves of the Tohoku mainshock. For the source in western Shikoku, the first tremor burst occurred during the arrivals of Love and Rayleigh waves between 350 and 450 s (Fig. 3). Additional tremor bursts with smaller amplitudes continued until 800 s (  Fig. S1 in the electronic supplement). In central Shikoku, clear tremor bursts were mainly associated with Rayleigh waves between 350 and 500 s, and smaller amplitude tremor bursts lasted until 700 s (  Fig. S1 in the electronic supplement). Study examining

Table 1
Summary of Tectonic Tremor around the World Triggered by the Tohoku Earthquake

Region	Tremor Locations Triggered by the Tohoku Earthquake				Notes	Previous Observations of Ambient and/or Triggered Tremor
	Longitude	Latitude	Assumed Depth (km)			
Alaska, U.S.	-146.06	61.67	45	Figure 6		* (Peterson and Christensen, 2009) † This study, (Flinchum and Brudzinski, 2011; Rubinstein <i>et al.</i> , 2011)
Aleutian Arc, U.S.	-166.26	53.97	45	Figure 5, central		* (Peterson <i>et al.</i> , 2011; Brown <i>et al.</i> , 2013) † This study and Rubinstein <i>et al.</i> , (2011)
	-166.90	53.59	45	Figure 5, western		
	-163.27	55.26	45	Figure 5, eastern		
Cascadia (Vancouver Island), Canada	-127.39	50.31	35	Figure 7		* (Rogers and Dragert, 2003; Gomberg and the Cascadia 2007 and Beyond Working Group, 2010) ‡ (Rubinstein <i>et al.</i> , 2007, 2009; Gomberg, 2010) † This study and Rubinstein <i>et al.</i> (2011)
Cascadia (southern Oregon), U.S.	-123.38	42.84	35	Figure 8		* (Wech and Creager, 2011) † This study, (Gonzalez-Huizar <i>et al.</i> , 2012)
Nankai (Shikoku), Japan	132.78	33.45	35	Figure 3, western		* (Obara, 2002, 2011) ‡ (Miyazawa and Brodsky, 2008; Miyazawa <i>et al.</i> , 2008) † This study
	133.24	33.83	35	Figure 3, eastern		
North Island of New Zealand	176.52	-39.15	45	Figure 11, southwest		* (Kim <i>et al.</i> , 2011; Ide, 2012) ‡ (Fry <i>et al.</i> , 2011) † This study
	176.76	-38.96	45	Figure 11, northeast		
Parkfield–Cholame section of the San Andreas fault (SAF), central California, U.S.	-120.31	35.76	25	Figure 9, see © Table S1 (available as an electronic supplement) for a detailed calculation of the average LFE location based on the LFE catalog in this region.		* (Nadeau and Dolenc, 2005; Nadeau and Guilhem, 2009; Shelly <i>et al.</i> , 2009) ‡ (Gomberg <i>et al.</i> , 2008; Peng <i>et al.</i> , 2009) † This study and Hill <i>et al.</i> (2013)
San Jacinto fault (SJF), southern California, U.S.	-116.64	33.58	25	Figure 10		‡ (Gomberg <i>et al.</i> , 2008; Chao, Peng, Fabian, <i>et al.</i> , 2012) † this study
Taiwan	120.88	23.05	25	Figure 4, south		* (Chao <i>et al.</i> , 2011) ‡ (Peng and Chao, 2008; Chao, Peng, Wu, <i>et al.</i> , 2012) † This study and Gonzalez-Huizar <i>et al.</i> (2012)
	121.43	24.27	25	Figure 4, north 1		
	121.85	24.61	25	Figure 4, north 2		

(continued)

Table 1 (Continued)

Region	Tremor Locations Triggered by the Tohoku Earthquake			Notes	Previous Observations of Ambient and/or Triggered Tremor
	Longitude	Latitude	Assumed Depth (km)		
Other Regions					
Armenia (Garni)				Possible triggered tremor event.	† (Gonzalez-Huizar <i>et al.</i> , 2012)
			Closest station: IU.GNI (longitude = 44.74, latitude = 40.15)		
Calaveras fault (CF), northern California, U.S.				No triggered tremor. ⑤ Figure S4 (available as an electronic supplement)	‡ (Gomberg <i>et al.</i> , 2008; Chao, Peng, Fabian, <i>et al.</i> , 2012)
			Closest station: BK.MHC (longitude = -121.64, latitude = 37.34)		
Costa Rica				Possible triggered tremor event. ⑤ Figure S3a (available as an electronic supplement)	* (Brown <i>et al.</i> , 2009; Outerbridge <i>et al.</i> , 2010) † This study
			Closest station: II.JTS (longitude = -84.95, latitude = 10.29)		
Cuba (Guantanamo)	-74.74	19.94	20	Clear triggered tremor event. East of CU.GTBY station	‡ (Gonzalez-Huizar <i>et al.</i> , 2012; Peng <i>et al.</i> , 2013) † (Peng <i>et al.</i> , 2013)
	-75.24	19.85	20	Clear triggered tremor event. West of CU.GTBY station	
Mexico (Guerrero)				No triggered tremor. ⑤ Figure S3b (available as an electronic supplement)	* (Payero <i>et al.</i> , 2008; Kostoglodov <i>et al.</i> , 2010) ‡ (Zigone <i>et al.</i> , 2012)
			Closest station: G.UNM (longitude = -99.18, latitude = 19.33)		
Queen Charlotte Margin, Canada				Clear triggered tremor event.	* (H. Kao, personal comm., 2012) ‡ (Aiken <i>et al.</i> , 2013) † (Aiken <i>et al.</i> , 2013)
			Closest station: CN.DIB (longitude = -132.48, latitude = 53.20)		
South Chile				No seismic station in this region is available during the Tohoku earthquake	* (Ide, 2012) ‡ (Peng <i>et al.</i> , 2012)
			Closest station: YJ.ISM01 (longitude = -73.83, latitude = -45.93)		

Observations of Ambient and/or Triggered Tremor in each region:

*Ambient tremor.

†Tremor triggered by the Tohoku earthquake.

‡Tremor triggered by other teleseismic earthquakes.

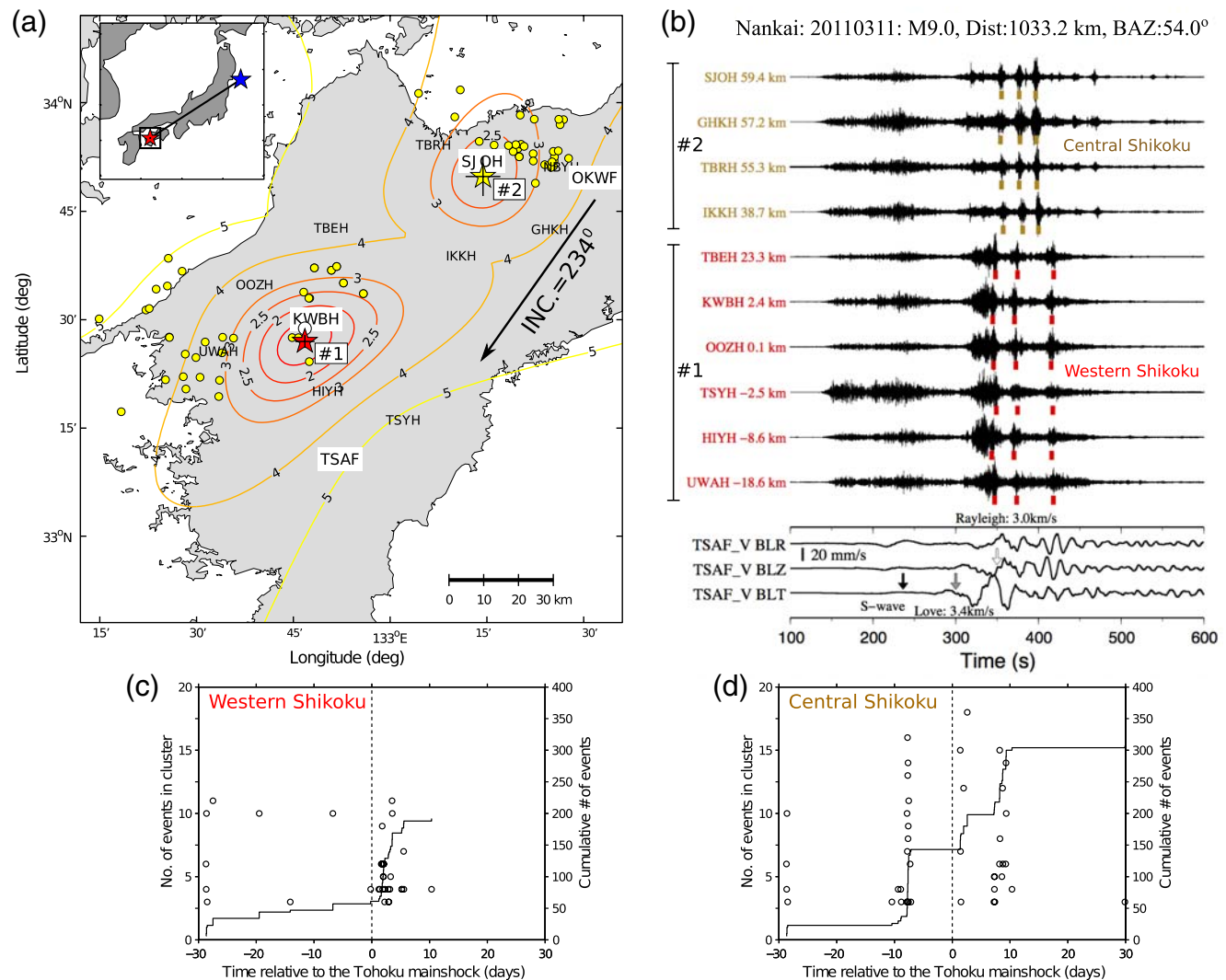


Figure 3. Triggered and ambient tremor observations in Shikoku, Nankai, around the occurrence time of the M 9.0 Tohoku mainshock. (a) Map of two sources of triggered tremor (stars) and seismic stations (marked by station names) in southwest Japan. The stations used in Figures 2 and 12 are marked with larger fonts. The contour lines denote the root-mean-square (rms) differences (in seconds) between the observed and predicted S -wave travel times of tremor bursts. The cross marks the error estimation of tremor location (star). The large circle indicates the location of tremor triggered by the 2008 M 7.9 Wenchuan earthquake (Miyazawa *et al.*, 2008). The small circles mark the ambient tremor locations (Obara *et al.*, 2010), one month before and after the Tohoku mainshock within 50 km from the epicenter of triggered tremor sources. The arrow marks the incident (INC.) direction of the incoming surface waves from the Tohoku mainshock, and the inset shows the great circle path between the mainshock and the study region (square). (b) The 5 Hz high-pass filtered seismograms in E-component showing the moveout of triggered tremor at multiple source regions in Shikoku. The along-strike distance to the tremor source in western Shikoku (Table S1 in the electronic supplement) and the station names are marked to the left of the seismograms. The tremor bursts used to locate different tremor sources (stars) shown in (a) are marked by vertical dotted lines with different numbers (i.e., Number 1 and Number 2). The bottom three traces show the instrument-corrected strong-motion velocity (V) seismograms in radial (BLR), vertical (BLZ), and transverse (BLT) components at the F-net station TSAF. The study region, magnitude (M) of the Tohoku mainshock, and the epicenter distance (Dist) and back azimuth (BAZ) relative to the station TSAF are shown above the seismograms. The zero time corresponds to the origin time of the Tohoku mainshock. The arrows mark the predicted arrivals of the S wave, the Love wave, and the Rayleigh wave from left to right. The thick vertical bar marks the amplitude scale of the surface waves. (c) The ambient tremor activity in western Shikoku one month before and after the mainshock shown in (a). Each open circle (left y axis) marks the number of events in each cluster in the ambient tremor catalog. The line (right y axis) shows the cumulative number of events within each cluster. (d) The ambient tremor activity in central Shikoku. Other notations are the same as in (c). The color version of this figure is available only in the electronic edition.

the relationship between triggered tremor and surface waves in this region is ongoing (Enescu *et al.*, 2012).

We also compare the triggered tremor sources with the ambient tremor locations (Obara *et al.*, 2010) one month be-

fore and after the Tohoku earthquake within 50 km of the epicenter of triggered tremor sources. As shown in Figure 3a, hourly ambient tremor generally occurred in the down-dip directions as compared with the triggered tremor. Even if

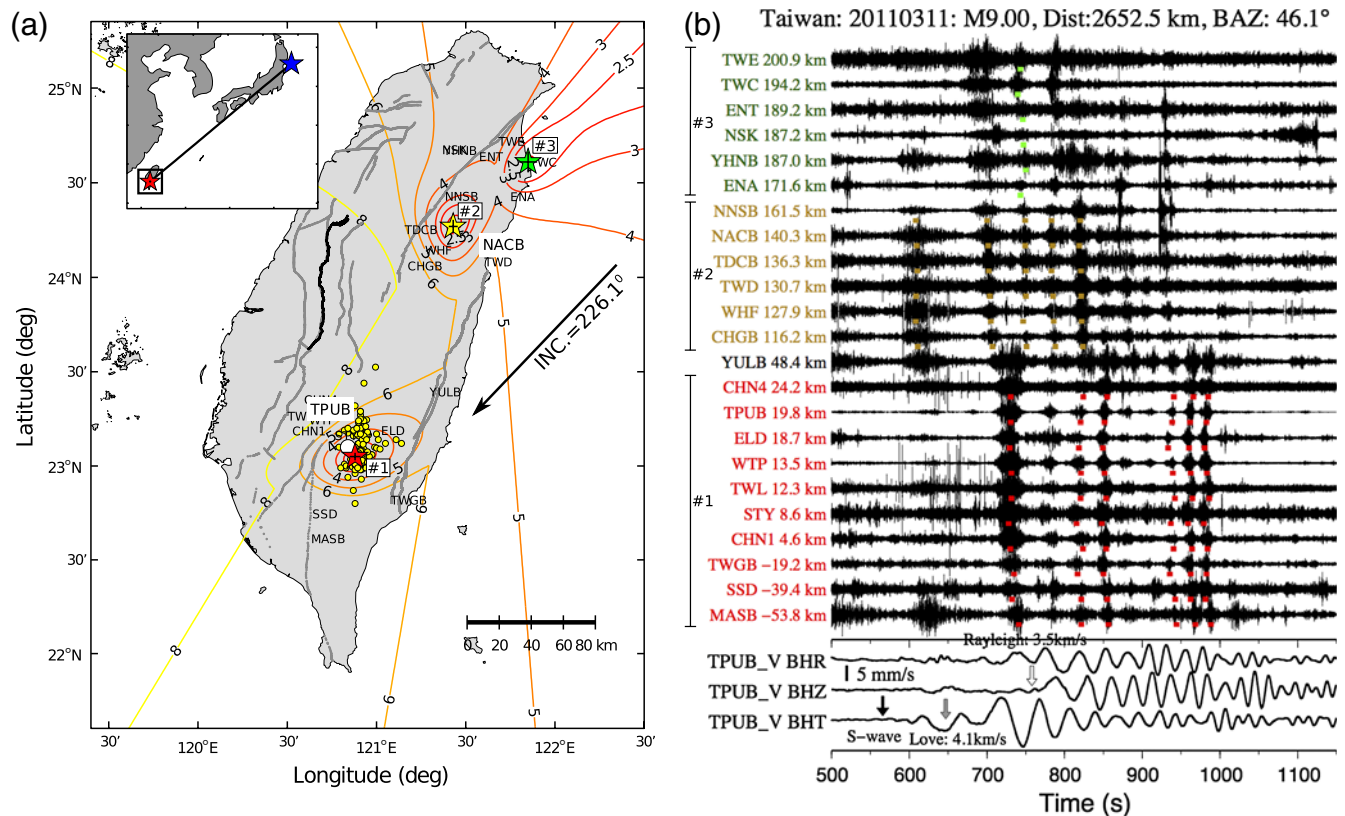


Figure 4. Triggered tremor observed in Taiwan. (a) Map of three sources of triggered tremor in Taiwan during the Tohoku earthquake. The small circles mark the locations of ambient tremor from February to April 2010 (Chao *et al.*, 2011). The large circle indicates the location of tremor triggered by the 2001 M 7.8 Kunlun earthquake (Peng and Chao, 2008). The thin and thick lines mark the active faults and the rupture zone of the 1999 M 7.6 Chi-Chi earthquake. Other notations are the same as in Figure 3a. (b) The 5 Hz high-pass filtered seismograms in the E-component showing the moveout of triggered tremor at multiple source regions in Taiwan. The seismograms are plotted along the strike of the Central Range. The bottom three traces show the instrument-corrected broadband velocity seismograms at station TW.TPUB. Other notations are the same as in Figure 3b. The color version of this figure is available only in the electronic edition.

we do not fix the triggered tremor depth at 35 km, the change in the best-fitting horizontal location is within $\pm 0.02^\circ$, which would still place the triggered tremor at the up-dip edge of the ambient tremor zone. In addition, ambient tremor activity in both regions shows slightly different temporal patterns before and after the Tohoku mainshock. In western Shikoku, while ambient tremor was not active before the Tohoku mainshock, tremor activity significantly increased after the mainshock (Fig. 3c). In central Shikoku, while ambient tremor episodes were active before the Tohoku mainshock, their occurrence rates did not significantly change after the mainshock (Fig. 3d). We note that no large amplitude-triggered tremor identified in the first 800 s was listed in the ambient tremor catalog (Obara *et al.*, 2010).

Taiwan

Triggered tremor has been found in the southern Central Range of Taiwan, an arc-continent collision environment (Peng and Chao, 2008; Tang *et al.*, 2010; Chao, Peng, Wu, *et al.*, 2012). Triggered tremor is mainly located in the lower crust below the seismogenic zone and above the Moho

(Tang *et al.*, 2010; Chao, Peng, Wu, *et al.*, 2012). However, it is still unclear whether it occurs on the low-angle detachment fault or the high-angle thrust fault beneath the Central Range. It has also been observed in the northern Central Range (Peng and Chao, 2008; Chao, Peng, Wu, *et al.*, 2012). However, accurate tremor locations and tremor-generation environments are still unclear because of a lack of high-quality recordings of tremor from many nearby stations. Recently, Chao *et al.* (2011) also found ambient tremor in the southern Central Range around the source regions of triggered tremor.

The Tohoku mainshock triggered at least three tremor sources in Taiwan (Fig. 4). The best-fitting tremor location in the southern Central Range is close to triggered tremor sources from previous studies (Peng and Chao, 2008; Tang *et al.*, 2010; Chao, Peng, Wu, *et al.*, 2012). As shown in Figure 4b, the strongest tremor burst occurred when the Love wave started at ~ 730 s and continued until 1000 s with subsequent Rayleigh waves. Two possible weak tremor bursts occurred between 620 and 680 s, and were recorded at stations TPUB, ELD, and WTP during the S wave and the beginning of the Love waves. In northern Taiwan, we identify two sources of triggered tremor close to previously identified

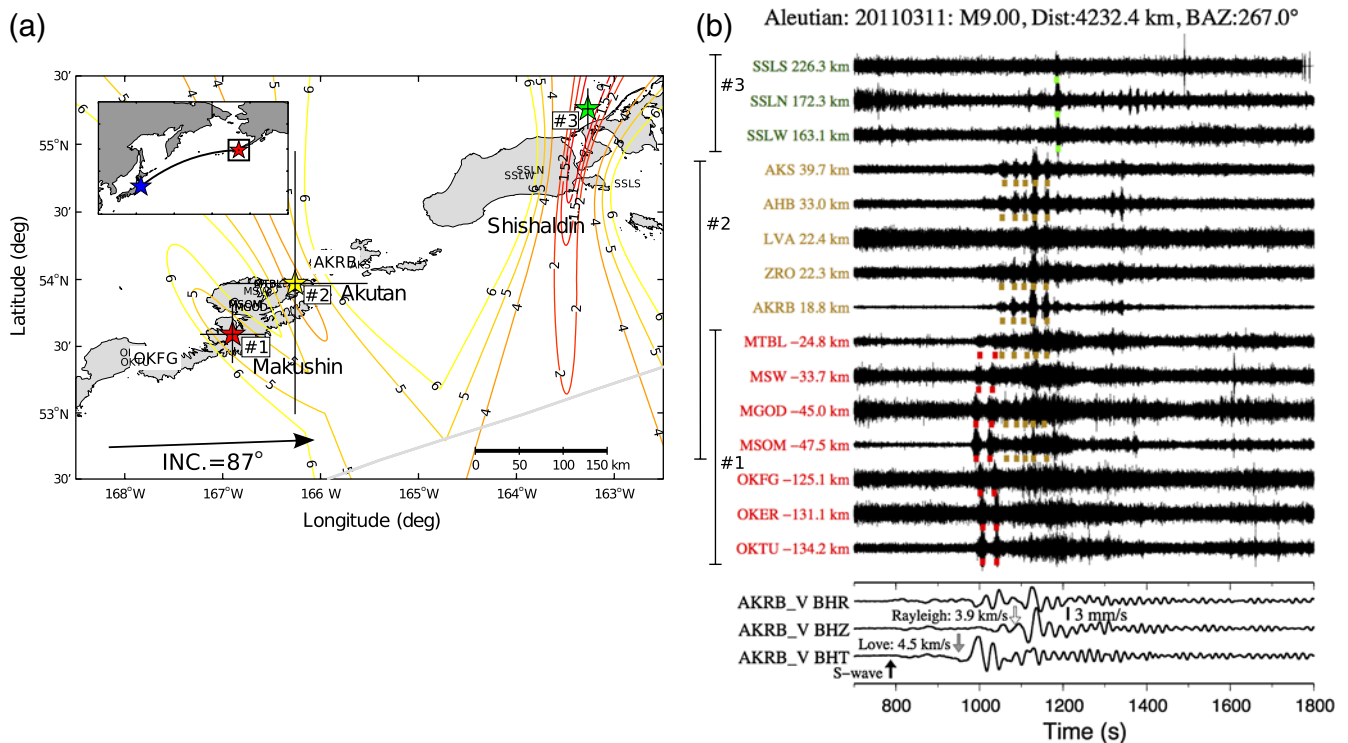


Figure 5. Triggered tremor observed in the Aleutian Arc. (a) Map of three sources of triggered tremor in the central Aleutian Arc during the Tohoku earthquake. The line without a number marks the subduction trench. The names of three volcanic islands are marked. Other notations are the same as in Figure 3a. (b) The 5 Hz high-pass filtered seismograms in the Z-component showing the moveout of triggered tremor at multiple source regions in the Aleutian Arc. The seismograms are plotted along the strike of the Aleutian Arc. The bottom three traces show the instrument-corrected broadband velocity seismograms at station AV.AKRB. Other notations are the same as in Figure 3b. The color version of this figure is available only in the electronic edition.

tremor locations (Chao, Peng, Wu, *et al.*, 2012). The first is beneath the northern Central Range near the broadband station NACB (Fig. 4a). A clear tremor burst occurred at ~ 600 s during the S wave and the beginning of the Love wave and continued up to ~ 950 s during the subsequent Love and Rayleigh waves. At another source farther north near the coast and around station TWC, tremor bursts occurred mainly between 700 and 800 s.

Aleutian Arc and Alaska

Ambient tremor occurred in south-central Alaska (Peterson and Christensen, 2009) and the Aleutian Arc (Peterson *et al.*, 2011; Brown *et al.*, 2013). In south-central Alaska, ambient tremor episodes mostly occur during slow-slip events (Peterson and Christensen, 2009), but no slow-slip events have been observed in the Aleutian Arc. In the central Aleutian Arc, the passing surface waves of the Tohoku mainshock generated three tremor sources near the volcano islands of Makushin, Akutan, and Shishaldin (Fig. 5), close to the main ambient tremor sources from the previous study (Peterson *et al.*, 2011). The first tremor source, located on the island of Makushin, occurred during the arrival of the Love wave between 1000 and 1050 s. The second tremor source was located between the Makushin and Akutan islands and occurred during the Rayleigh waves between 1050 and

1200 s. The third tremor source was triggered farther northeast near Shishaldin volcanic island during the passing Rayleigh waves at around 1200 s.

Flinchum and Brudzinski (2011) and Rubinstein *et al.* (2011) identified tremor beneath south-central Alaska triggered by the Tohoku earthquake. We further examine the source of triggered tremor in this region. A small-amplitude tremor burst occurred at ~ 1300 s during the arrival of the Love waves (Fig. 6). Subsequent Rayleigh waves triggered high-amplitude tremor bursts between 1400 and 2200 s. Triggered tremor was located near station KLU east of the region where previous ambient tremor was found (*i.e.*, around station SAW; Peterson and Christensen, 2009). It is also possible that additional tremor (note the different tremor signals at station RC01) might be triggered in the surrounding regions. However, because these regions contain only eight seismic stations, some as far as 400 km away from the tremor source, we do not have enough seismic station recordings to locate them accurately.

Cascadia

One of the most well-studied regions with episodic tremor and slip (ETS) is the Cascadia subduction zone (Gomberg and the Cascadia 2007 and Beyond Working Group, 2010; Beroza and Ide, 2011). In northern Cascadia,

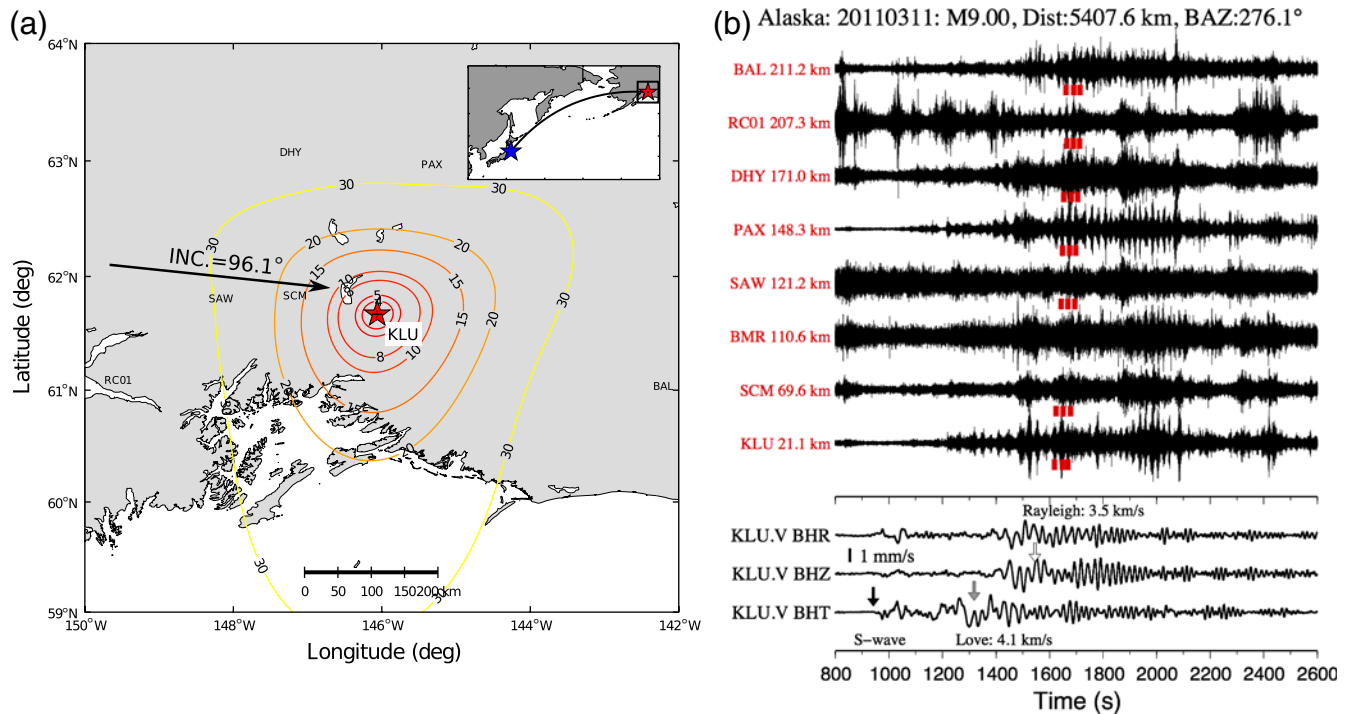


Figure 6. Triggered tremor observed in south-central Alaska. (a) Map of the triggered tremor source in south-central Alaska during the Tohoku earthquake. Other notations are the same as in Figure 3a. (b) The 5 Hz high-pass filtered seismograms in the E-component showing the moveout of triggered tremor at multiple source regions in the Aleutian Arc. The seismograms are aligned with the epicentral distance relative to the best tremor source. The bottom three traces show the instrument-corrected broadband velocity seismograms at station AK.-KLU. Other notations are the same as in Figure 3b. The color version of this figure is available only in the electronic edition.

ETS occurs every 14.5 ± 1 months and lasts for about 2–3 weeks (Miller *et al.*, 2002; Rogers and Dragert, 2003; Gomberg and the Cascadia 2007 and Beyond Working Group, 2010; Wech and Creager, 2011). Triggered tremor has also been observed beneath Vancouver Island in northern Cascadia (Rubinstein *et al.*, 2007, 2009) and the Cascadia subduction zone in central Washington (Gomberg, 2010). Following the 2011 Tohoku earthquake, triggered tremor was identified near Vancouver Island (Rubinstein *et al.*, 2011) and southern Oregon (Gonzalez-Huizar *et al.*, 2012). Figure 7 shows the location and waveforms of a Tohoku-triggered tremor in northern Vancouver Island. The tremor, which occurred near station MAYB, was close to the source regions of previously identified triggered tremor sources (Rubinstein *et al.*, 2007, 2009). As found in other regions, the tremor first occurred during the arrival of the Love wave at ~ 1600 s, and was further modulated by subsequent Rayleigh waves.

We compare the ambient tremor activity one month before and after the Tohoku mainshock (Fig. 7c) as listed in the Source-Scanning Algorithm (SSA) tremor catalog (Kao and Shan, 2004; Kao *et al.*, 2010). Triggered tremor was located further towards the trench as compared with the ambient tremor locations (Fig. 7a). In addition, the ambient tremor in this region was sporadic with bursts of activity at 29 and 4 days before the occurrence of the Tohoku mainshock. There was a clear increase in the number of tremor

episodes starting a few hours after the Tohoku mainshock. Additional tremor episodes occurred about 9 days after the mainshock. We also examine the tremor activities listed in the Waveform Envelope Correlation and Clustering catalog (WECC; Wech and Creager, 2008; Wech, 2010) during the same time period, and find that most of them occurred in the southern portion of Vancouver Island. According to this catalog, there was no ambient tremor a few days before and after the Tohoku mainshock (Fig. 7d).

In southern Oregon, clear tremor bursts occurred during the Love and Rayleigh waves recorded at station HUMO (Gonzalez-Huizar *et al.*, 2012), and other nearby stations (Fig. 8). Weak tremor signals appeared to start right after the teleseismic *S* wave and became further intensified during the subsequent long-period Love (~ 1700 – 1900 s) and Rayleigh waves (~ 2000 – 2200 s). Tremor continued to be modulated by the short-period Rayleigh waves up to ~ 3000 s. We are able to identify nine coherent tremor peaks at three nearby stations and the average tremor location is close to station K02D. We also examine the ambient tremor activities (Wech and Creager, 2008; Wech, 2010) one month before and after the Tohoku mainshock, and find that no tremor occurred within a few days around that mainshock. In addition, the triggered tremor appears to locate just outside a cluster of ambient tremor. A tremor observed at station L04D had different moveout with the rest stations, suggesting a possible new source region. In contrast, no clear triggered tremor took

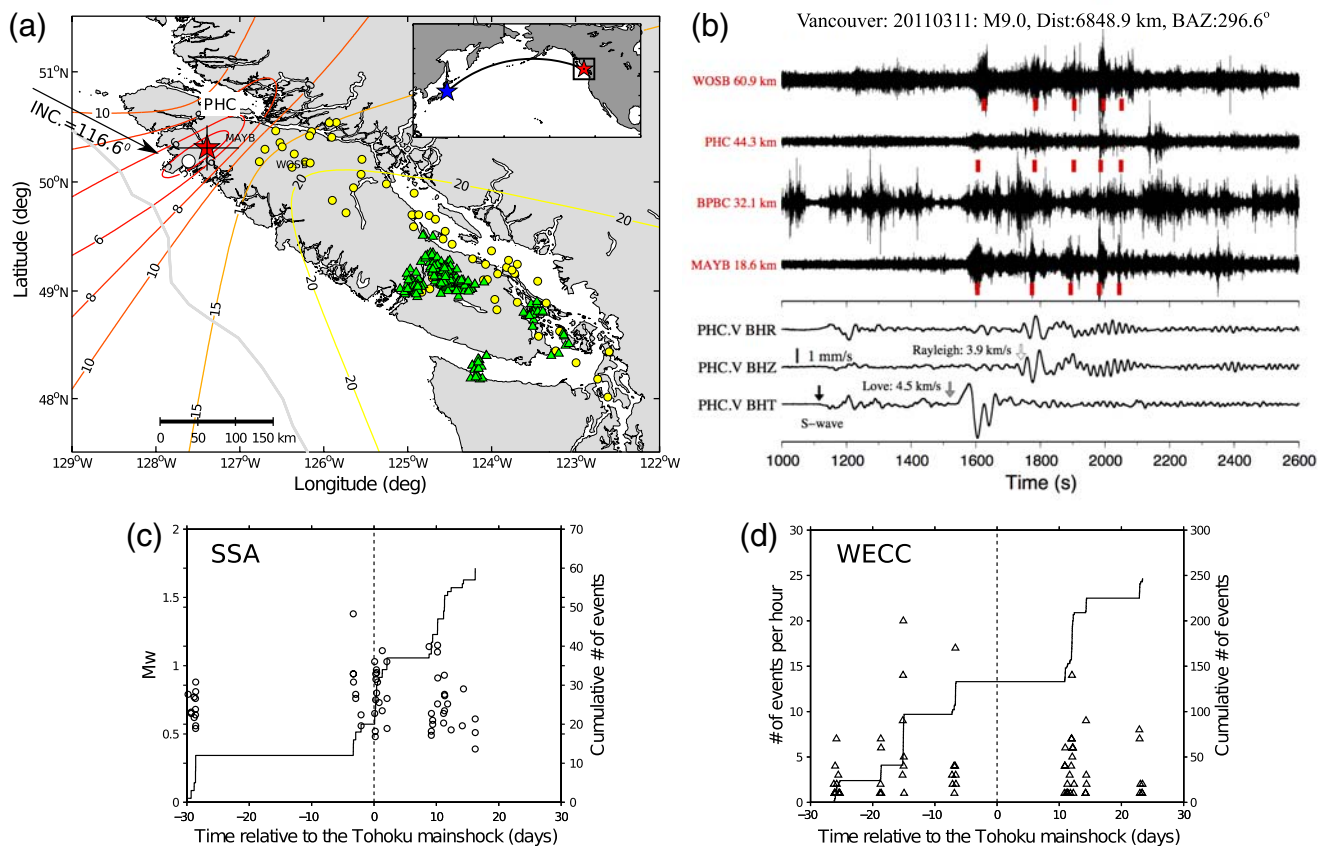


Figure 7. Triggered and ambient tremor in northern Vancouver Island around the occurrence time of the Tohoku mainshock. (a) Map of the triggered tremor source in northern Vancouver Island during the Tohoku earthquake. The large circle marks the location of tremor triggered by the 2002 M 7.8 Denali, Alaska, earthquake (Rubinstein *et al.*, 2007). The small circles mark the locations of ambient tremor one month before and after the Tohoku mainshock listed in the Source-Scanning Algorithm (SSA) tremor catalog (Kao and Shan, 2004; Kao *et al.*, 2010). The small triangles show ambient tremor locations during the same period listed in the Waveform Envelope Correlation and Clustering (WECC) tremor catalog (Wech and Creager, 2008; Wech, 2010). Other notations are the same as in Figure 3a. (b) The 5 Hz high-pass filtered seismograms in the Z-component showing the moveout of triggered tremor for a single tremor source. The seismograms are aligned with the epicentral distance relative to the best tremor source. The bottom three traces show the instrument-corrected broadband velocity seismograms at station CN.PHC. Other notations are the same as in Figure 3b. (c) Ambient tremor activity on Vancouver Island one month before and after the Tohoku mainshock from the SSA tremor catalog. The left y-axis shows the moment magnitude of each tremor, and the line shows the cumulative number of tremor instances. (d) Ambient tremor activity one month before and after the Tohoku mainshock from the WECC tremor catalog. The color version of this figure is available only in the electronic edition.

place in central Cascadia (© Fig. S2 in the electronic supplement).

Parkfield, Central California

The Parkfield–Cholame section of the SAF in central California is another region where ambient (Nadeau and Dolenc, 2005; Nadeau and Guilhem, 2009; Shelly *et al.*, 2009; Shelly and Hardebeck, 2010) and triggered (Gomberg *et al.*, 2008; Peng *et al.*, 2009, 2010; Shelly *et al.*, 2011) tremors have been well studied. Rather than locating the tremor with our envelope cross-correlation technique, we take advantage of the existing LFE catalog (Shelly and Hardebeck, 2010) and use the LFEs during teleseismic waves to quantify spatiotemporal evolutions of the triggered tremor.

Hill *et al.* (2013) conducted a detailed analysis of the tremor around Parkfield, triggered by the 2011 Tohoku main-

shock. Here, we briefly summarize their observations. A weak tremor burst was first triggered at ~ 1400 s by the arrival of an S wave and the tremor source was located in the creeping section of the SAF, northwest of station PKD (Fig. 9). A weak tremor burst triggered by the SHSH wave (e.g., an SH wave reflected by the Earth's surface midway between the epicenter and Parkfield) at ~ 1600 s was located beneath the hypocenter of the 2004 M_w 6.0 Parkfield earthquake. Afterwards, the Love wave triggered two tremor bursts near Cholame, at about 1800 and 1950 s, respectively. The subsequent Rayleigh waves also triggered multiple tremor sources scattered in both the creeping section of the SAF and around Cholame. As with similar other regions, we further examined ambient tremor six days before and after the Tohoku mainshock. As shown in Figure 9b, clear tremor episodes occurred 2, 4, and 6 days before the Tohoku mainshock, and tremor activity clearly increased during the

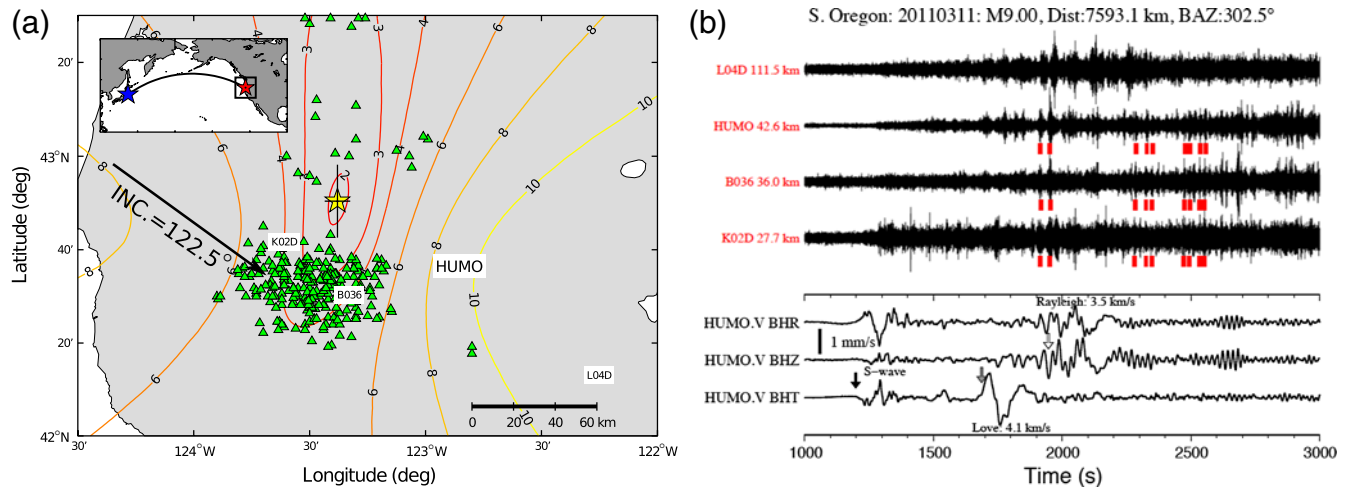


Figure 8. Triggered tremor in southern Oregon. (a) Map of triggered tremor during the Tohoku earthquake. The small triangles show ambient tremor locations listed in the WECC tremor catalog one month before and after the Tohoku mainshock. Other notations are the same as in Figure 3a. (b) The 5–15 Hz band-pass filtered seismograms showing the moveout of triggered tremor. The seismograms are aligned with the epicentral distance relative to the best tremor source. The bottom three traces show the instrument-corrected broadband velocity seismograms at station BK.HUMO. Other notations are the same as in Figure 3b. The color version of this figure is available only in the electronic edition.

teleseismic waves and in the first few hours afterwards. However, we did not find any significant changes in tremor activities a few days after the mainshock.

San Jacinto Fault, Southern California

The 2002 M_w 7.9 Denali fault earthquake is the only teleseismic event previously observed to have triggered tremor along the SJF in southern California (Gomberg *et al.*, 2008; Chao, Peng, Fabian, *et al.*, 2012). In addition, although several studies have attempted to identify ambient and additional triggered tremor in this region (Hillers and Ampuero, 2009), ambient tremor has not been detected with current instrumentation (J. Ampuero, personal comm., 2011).

Here we identify possible tremor triggered at the SJF during the passing surface waves of the Tohoku earthquake. We first examine spectrograms (Peng *et al.*, 2011) of several recordings at broadband stations RDM, KNW, and CRY and determine that tremor signals are best shown in the horizontal component with a frequency range of 4–10 Hz. The first tremor burst occurred during the Love wave at \sim 2050 s. Additional tremor bursts occurred between 2350 and 2550 s during the later-arriving Rayleigh waves (Fig. 10). In addition, a local earthquake occurred at \sim 2240 s during the first few cycles of the Rayleigh waves. The tremor during the Tohoku surface waves was located in the Anza section of the SJF, about \sim 36 km southeast of the tremor source triggered by the Denali fault earthquake (Gomberg *et al.*, 2008).

North Island, New Zealand

The Hikurangi Subduction Margin, New Zealand, marks the convergent plate boundary where the Hikurangi Plateau, part of the Pacific plate, subducts beneath the North Island at

2–6 cm/yr (Wallace *et al.*, 2004). Numerous slow-slip events have been observed both in the up- and down-dip directions from the interseismically locked regions (McCaffrey *et al.*, 2008; Wallace and Beavan, 2010). Delahaye *et al.* (2009) conducted a systematic search but failed to find any tremor signals associated with shallow slow-slip events at the northern Hikurangi margin. Instead, they found numerous reverse-faulting microearthquakes. Recently, triggered (Fry *et al.*, 2011) and ambient (Kim *et al.*, 2011; Ide, 2012) tremor have been found in the North Island of New Zealand, near the regions of deep slow-slip events (Wallace and Beavan, 2010). In addition, ambient tremor has been observed on the Alpine fault in the South Island (Wech *et al.*, 2012). The Tohoku mainshock also triggered clear tremor bursts at stations BKZ and BHHZ (Fig. 11), mostly during the passing Rayleigh waves between 2650 and 2900 s. The tremor source is located southeast of Lake Taupo, which is about 60 km northeast of the tremor source triggered by the 2010 M_w 8.8 Chile mainshock (Fry *et al.*, 2011). In general, these triggered tremor sources occurred around ambient tremor (Ide, 2012) and aligned parallel to the subduction zone trench.

Other Regions

Ambient tremor and episodic slow-slip events have been found along the Middle–American Trench in Guerrero, Mexico (Payero *et al.*, 2008) and in Costa Rica (Brown *et al.*, 2009; Outerbridge *et al.*, 2010; Walter *et al.*, 2011). Tremor triggered by the 2010 M_w 8.8 Chile earthquake was found in Guerrero, but no clear triggered tremor was identified in that region during the 2011 Tohoku earthquake (Zigone *et al.*, 2012). In addition, so far, no triggered tremor has been found in Costa Rica (Swiecki and Schwartz, 2010). We find possible high-frequency bursts that coincide with the arrival of

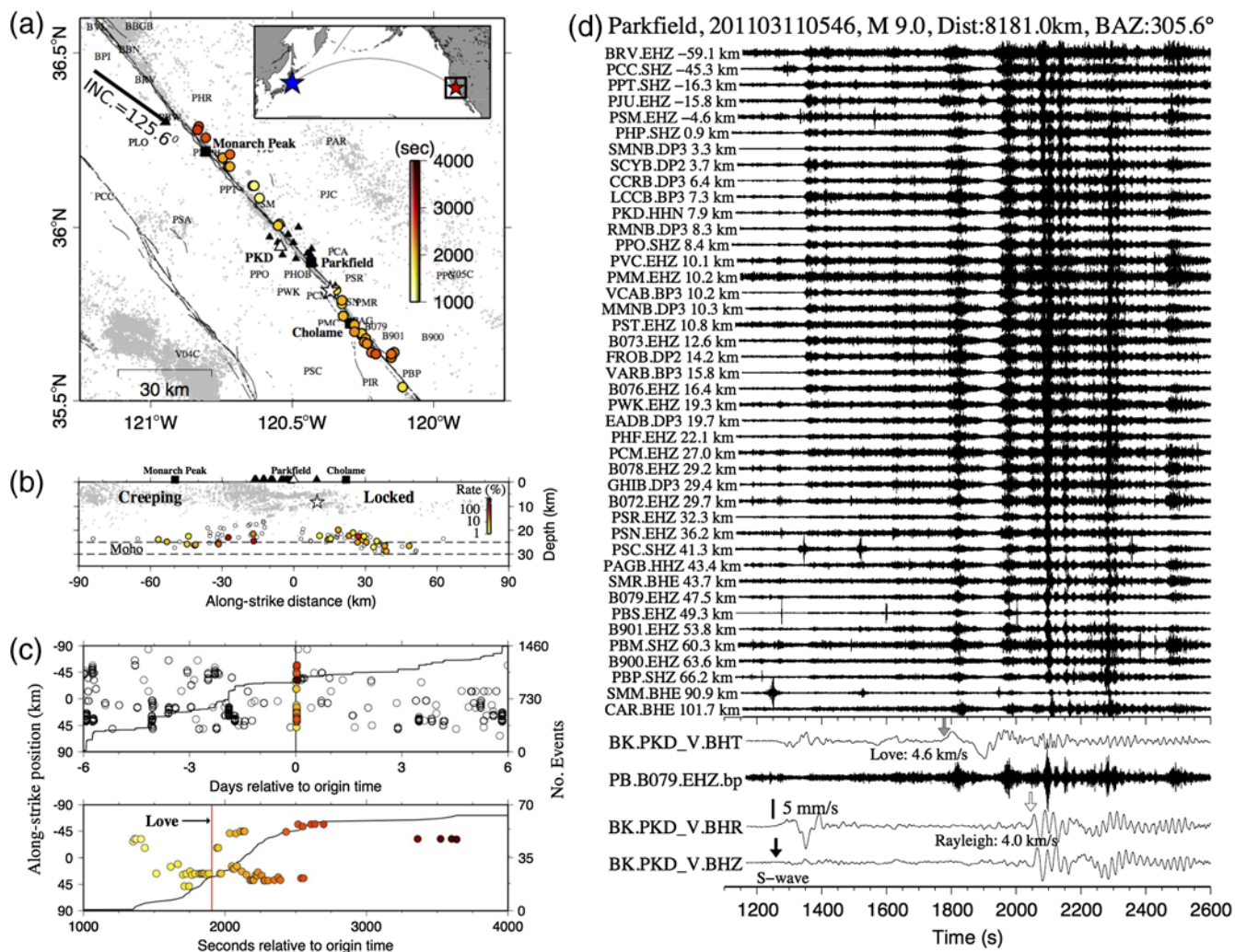


Figure 9. Triggered and ambient tremor along the Parkfield–Cholame section of the San Andreas fault (SAF) around the Tohoku mainshock occurrence time. (a) Map of triggered tremor during the Tohoku mainshock. The tremor locations are marked as circles denoting the time since the mainshock. The small points mark the background seismicity, and the lines denote active faults. Other notations are the same as in Figure 3a. (b) An along-fault cross-section view showing the depth profile of the 88 tremor locations. The scale numbers denote the ratio between the number of tremor occurrences during the teleseismic surface waves to the total number of tremor occurrences within the six days prior to the Tohoku mainshock. (c) (top) Along-strike distances versus the number of tremor occurrences within the six days before and after the Tohoku mainshock (bottom). A zoom-in plot around the teleseismic waves of the mainshock. The vertical line marks the arrival time of large-amplitude Love waves. (d) The 2–8 Hz band-pass filtered seismograms showing the moveout of triggered tremor at multiple sources. The seismograms are plotted along the SAF strike. The bottom three traces show the instrument-corrected broadband velocity seismograms at station BK. PKD. Other notations are the same as in Figure 3b. The color version of this figure is available only in the electronic edition.

Love waves at the broadband station JTS in Costa Rica (© Fig. S3 in the electronic supplement). However, we could not confirm the existence of a triggered tremor based only on a single-station record. We also examined seismic recordings in the CF in northern California, where the 2002 Denali fault earthquake has triggered tremor (Gomberg *et al.*, 2008; Chao, Peng, Fabian, *et al.*, 2012), but have not found any clear triggering during the Tohoku mainshock (© Fig. S4 in the electronic supplement).

Gonzalez-Huizar *et al.* (2012) reported triggered tremor at station SAO in the creeping section of the SAF, station GNI in Armenia, station HUMO in south Oregon, and station

GTBY in Cuba. Because station SAO is only ~88 km away from the northwesternmost tremor on the creeping section of the SAF, it is not clear whether the recorded tremor signals originated from a new source region or if they could have been generated by the same source from the Parkfield–Cholame section, as shown in Figure 9. The 2011 Tohoku event has triggered tremor-like signals at station GNI in Armenia. Because the number of stations that recorded the tremor does not meet our selecting criterion (i.e., not recorded by at least three nearby stations in Armenia), we cannot say with the same level of certainty that these represent triggered tremor, nor can we accurately locate them. The

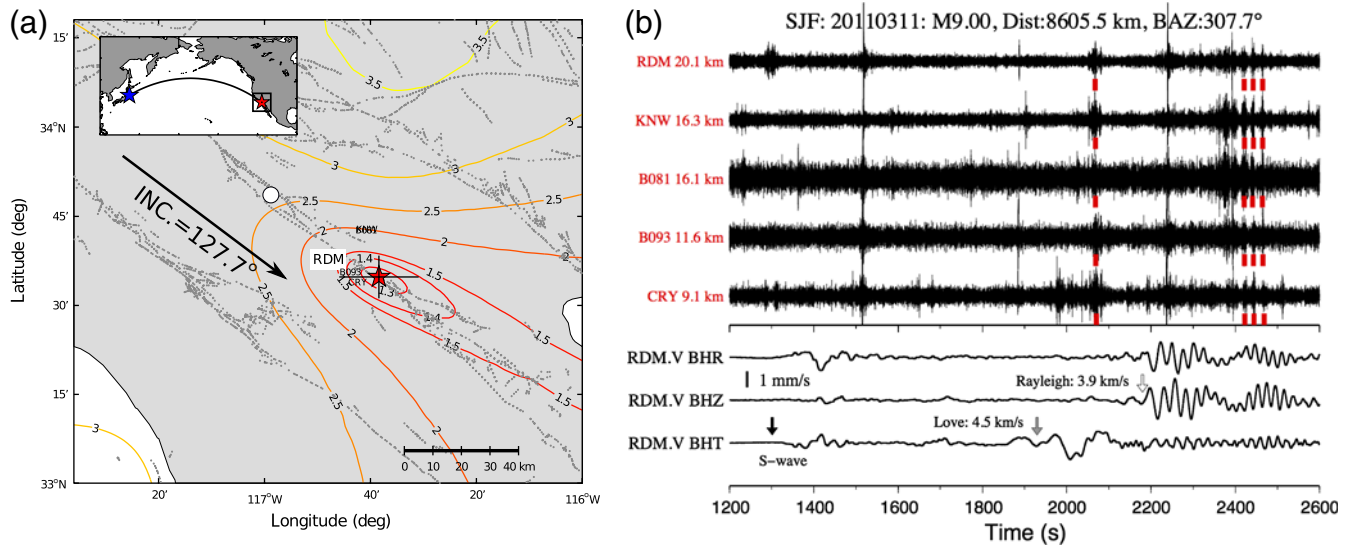


Figure 10. Triggered tremor observed at the San Jacinto fault (SJF) in southern California. (a) Map of the single triggered tremor source during the Tohoku earthquake. The large circle indicates the location of tremor triggered by the 2002 M 7.8 Denali fault earthquake (Gomberg *et al.*, 2008). Other notations are the same as in Figure 3a. (b) The 4–10 Hz band-pass filtered seismograms in the N-component showing the moveout of triggered tremor. The seismograms are aligned with the epicentral distance relative to the best tremor source. The bottom three traces show the instrument-corrected broadband velocity seismograms at station AZ.RDM. Other notations are the same as in Figure 3b. The color version of this figure is available only in the electronic edition.

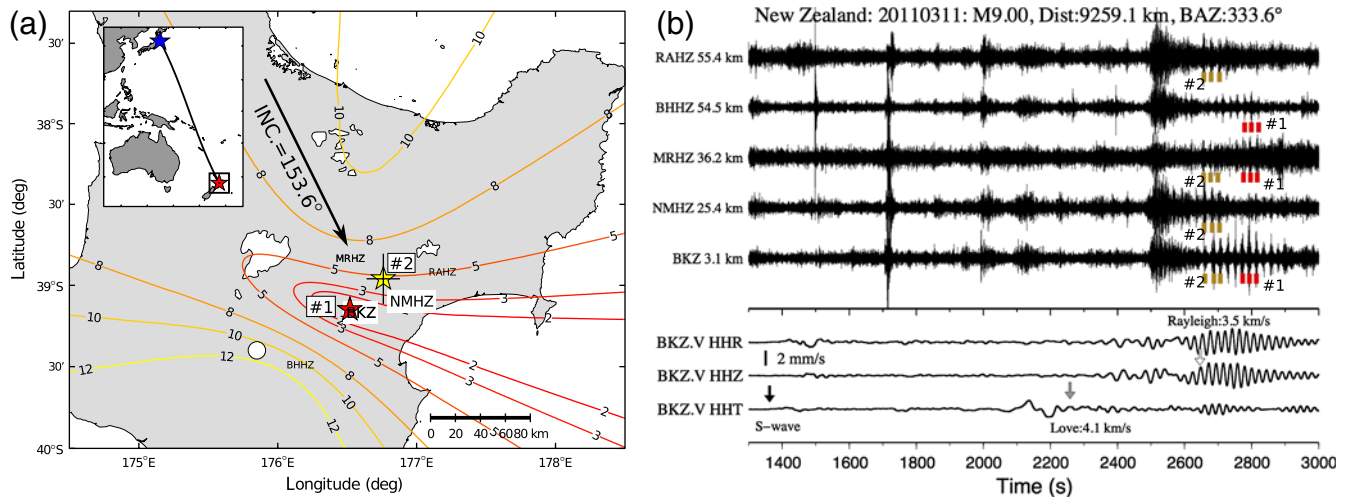


Figure 11. Triggered tremor observed in the North Island of New Zealand. (a) Map of triggered tremor during the Tohoku earthquake. The large circle indicates the location of tremor triggered by the 2010 M 8.8 Chile earthquake (Fry *et al.*, 2011). Other notations are the same as in Figure 3a. (b) The 2–8 Hz band-pass filtered seismograms in the E-component showing the moveout of triggered tremor. The seismograms are aligned with the epicentral distance relative to the best tremor source by station BKZ. The bottom three traces show the instrument-corrected broadband velocity seismograms at station NZ.BKZ. Other notations are the same as in Figure 3b. The color version of this figure is available only in the electronic edition.

2010 M_w 8.8 Chile earthquake and its large aftershocks also triggered tremor in Cuba (Gonzalez-Huizar *et al.*, 2012). By examining regional seismic network data during the Tohoku earthquake, Peng *et al.* (2013) identified at least two triggered tremor sources near the left-lateral Oriente fault. From these findings, we include only the Cuba case in a subsequent analysis in Figures 12 and 13.

Tremor Amplitudes and Dynamic Stress Changes

In this section we quantify the relationship between tremor amplitudes and dynamic stress changes in all 13 regions that we have examined in this study. In regions with multiple tremor sources (e.g., Japan, Taiwan, the Aleutian Arc), we measure the values for each tremor source separately.

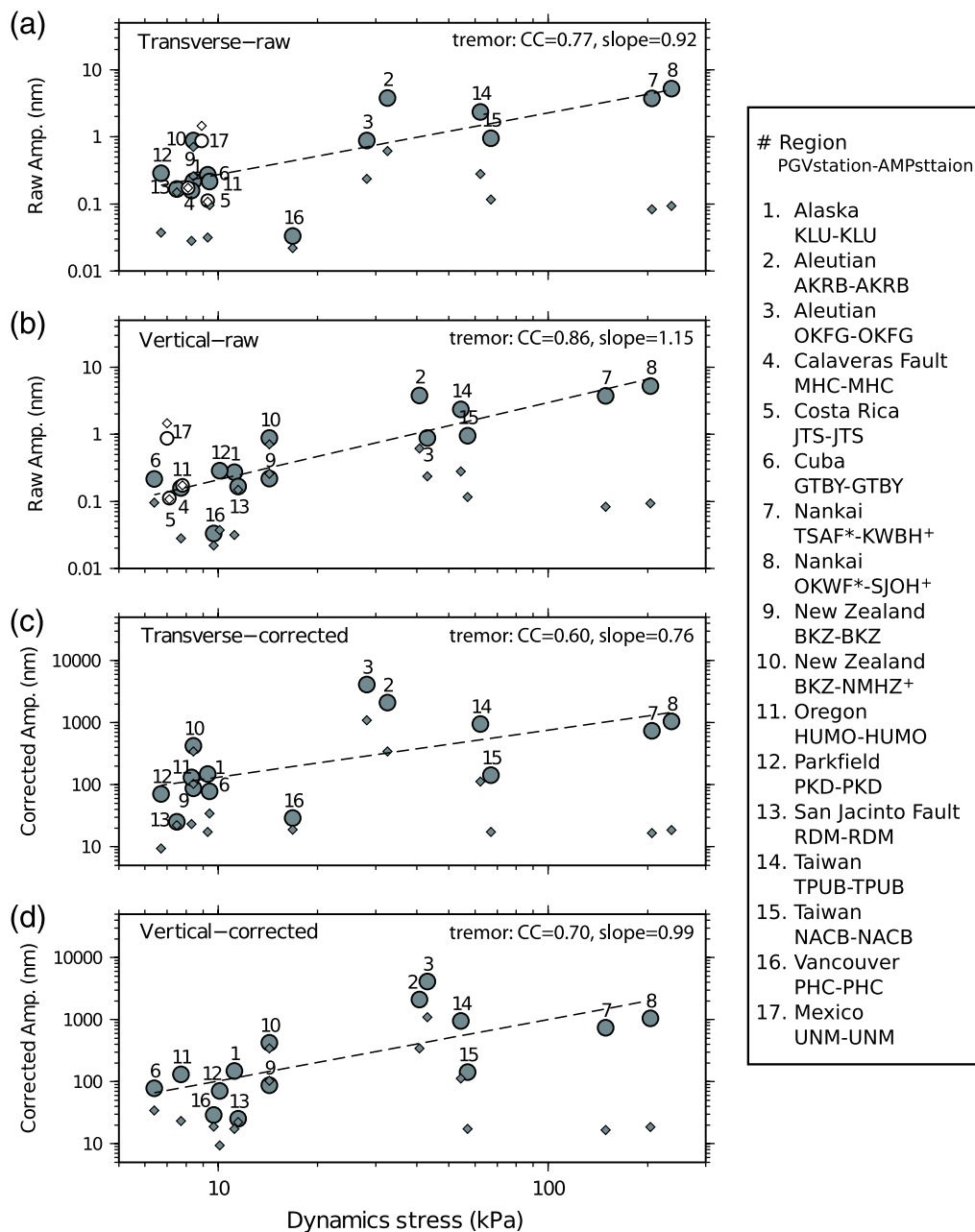


Figure 12. Median tremor amplitude measured from the 5–15 Hz two-horizontal-component displacement band-pass-filtered envelope functions versus the dynamic stress of surface waves for the Tohoku mainshock. Panels (a) and (b) show raw tremor amplitudes, and panels (c) and (d) show the amplitudes after correcting for geometrical spreading and attenuation. Tremor-triggering and nontriggering events are marked by shaded and open symbols, respectively. The background noise level, indicated by diamond symbols, is calculated from a 600-s time window before the occurrence of the Tohoku mainshock in each region. The numbers mark different regions (with their corresponding seismic stations used for measuring the peak ground velocity (PGV), and the station used for measuring the median amplitude of tremor and nontremor signals). The station names marked with an asterisk (*) and a cross (+) indicate strong-motion sensors (BL) and extremely short-period (EH) instruments, respectively (see Table S2 in the electronic supplement, for detailed instrument descriptions). Others are measured from broadband stations (BH or HH). The correlation coefficient (CC) and the slope of the fitting line are calculated for the median tremor amplitudes and corresponding dynamic stresses (shaded circles). The color version of this figure is available only in the electronic edition.

As mentioned before, the PGV is measured as the maximum peak on the transverse and vertical components of velocity seismograms within the apparent velocities of 5 to 2 km/s. To measure tremor amplitude, we follow our previous studies

(Chao, Peng, Fabian, *et al.*, 2012; Chao, Peng, Wu, *et al.*, 2012) and compute the median amplitude of triggered tremor from the two horizontal-component band-pass-filtered displacement seismograms during large-amplitude surface

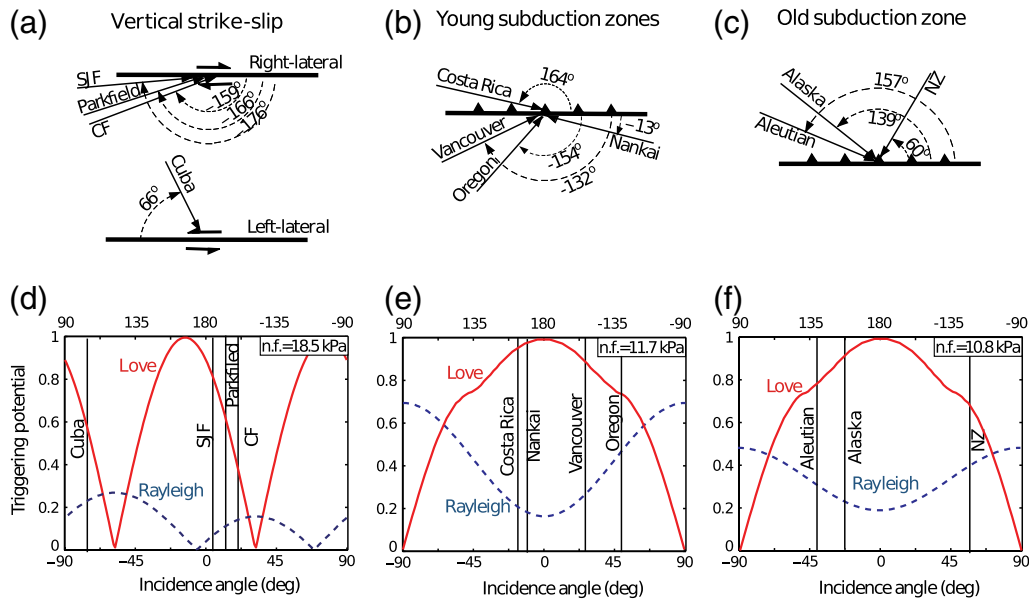


Figure 13. Surface-wave triggering potentials for three simplified tectonic models. Panels (a), (b), and (c) show idealized maps for the tectonic models, and the arrows represent the surface-wave incident angles relative to the strike of the major faults in each region. Panels (d), (e), and (f) show the normalized triggering potential of the Love (solid lines) and Rayleigh (dash lines) waves as a function of the incident angles for the tectonic models in (a), (b), and (c), respectively. The normalization factor (n.f.) is shown for each plot. Vertical lines in the triggering potential plots define the incident angle for each of the regions where tremor was triggered. The color version of this figure is available only in the electronic edition.

waves. To ensure that the tremor amplitudes at different sites are comparable, we use a fixed frequency range between 5–15 Hz. Because the median triggered tremor amplitude is not sensitive to the choice of the frequency range (2–8 Hz or 5–15 Hz), we chose 5–15 Hz to avoid the contamination of aftershock signals from the Tohoku mainshock rupture zone, especially in the Nankai region. Displacement seismograms were integrated from the band-pass-filtered velocity seismograms for the purpose of amplitude correction as described below. In regions with no triggered tremor, we measure the median amplitudes of 5–15 Hz band-pass-filtered seismograms during the surface-wave time period within the apparent velocities of 5–2 km/s. Finally, we compute the median amplitudes of the background noise during the 600 s before the arrival of the P wave of the mainshock.

We correct for the effects of geometrical spreading (Boore, 2003) and attenuation (Shearer, 1999; Chao, Peng, Fabian, *et al.*, 2012) with the following equation:

$$A_{\text{station}} = (A_{\text{source}}/R) \times \exp[(-2\pi f R)/(2V_S Q)], \quad (3)$$

where A_{station} is the observed tremor amplitude at a station, A_{source} is the amplitude at the tremor source (referred to as “corrected tremor amplitude”), R is the hypocentral distance between a station and the tremor source, $1/R$ is the geometrical spreading function (for $R < 70$ km), f is the dominant frequency, V_S is the shear-wave velocity, and Q is a quality factor. Here we assume constant $Q = 100$ and average $V_S = 3.9$ km/s for the lower crust (Shearer, 1999) and assume

$f = 6$ Hz with the highest amplitude of triggered tremor (Rubinstein *et al.*, 2007).

As shown in Figure 12, the median tremor amplitudes positively correlate with the dynamic stresses estimated from both Love and Rayleigh waves on the transverse and vertical components, respectively (Fig. 12). The correlation coefficient (CC) in the log–log scale is more than 0.60 for measurements both before and after the amplitude corrections. The corresponding two-tailed p value is 0.023, indicating that the correlation is significant at a 95% confidence level. In comparison, background noise does not show any correlation with dynamic stress.

Modeling of Tremor Triggering Potential

To quantify the triggering capability of surface waves from the Tohoku earthquake in different regions, we follow the modeling approach used by Hill (2008, 2010, 2012a,b) and Gonzalez-Huizar and Velasco (2011) for triggered earthquakes. Assuming shear faulting at nearby major plate-boundary faults is responsible for generating tremor signals, we use two modeling approaches that follow a simple Coulomb failure criterion. In the first approach, we estimate the capability of surface waves with fixed amplitude and frequency to trigger tremor on a fault plane with a specific orientation and faulting mechanism. In the second approach, we use time-dependent frequency and amplitude information of the triggering wave to model time-dependent dynamic stresses or stress grams.

First, we compute the triggering potential $P(\gamma)$ as the amplitude of the stress orbit projected onto the normal of the Coulomb failure envelope (equivalent to the dynamic Coulomb Failure Function, ΔCFF) and normalized by the maximum radius (semimajor axis) for the suite of orbits spanning all incidence angles γ of the incoming waves (Hill, 2012b). The null and maximum triggering potential is 0 and 1, respectively. Here we assume a predominant period of 20 s for both Love and Rayleigh waves. We use the same elastic and velocity parameter values defined in table 1 of Hill (2012a), a coefficient of static friction of 0.2, and a Skempton coefficient equal to 0.8. As stated above, we group our study regions into three tectonic models. For strike-slip faults (e.g., SAF and SJF), we use a vertical fault and set the tremor depth at 25 km. For the relatively young subduction zones (e.g., southwest Japan and Cascadia), we use a 15° shallow dipping fault and set the tremor depth at 35 km. For the relatively old subduction zones (e.g., Aleutian Arc, Alaska, and New Zealand), we use a 25° dipping angle to approximate the subduction-zone plate interface, and set the tremor depth at 45 km (e.g., Brown *et al.*, 2013). Because the faulting style for tremor in Taiwan is still not clear (Tang *et al.*, 2010; Chao, Peng, Wu, *et al.*, 2012), we do not include the results from Taiwan in this analysis.

Figure 13 shows the triggering potentials for Love and Rayleigh waves for each of the simplified tectonic models. For strike-slip faults (Fig. 13a,d), Love waves show a higher triggering potential than Rayleigh waves for the incident direction parallel to the strike of each tectonic region. This finding indicates that we should expect more predominant tremor activity while Love waves are passing, which is generally consistent with observations at Parkfield (Fig. 9) and along the SJF (Fig. 10). However, Rayleigh waves triggered larger amplitude tremor than Love waves in Parkfield (Fig. 9) and in Cuba (Peng *et al.*, 2013). For the relatively young subduction zones (Fig. 13b,e), Love waves have a much higher triggering potential than Rayleigh waves for the incident angles of interest. Thus, we expect triggered tremor bursts with high amplitudes during the arrival of Love waves, which were observed in these regions (e.g., Figs. 3 and 7). Finally, for the relatively old subduction zones model (Fig. 13c,f), Love waves still show higher triggering potential. In this case, we expect higher amplitudes in triggered tremor rates during Love waves than during Rayleigh waves (e.g., Fig. 5). Overall, the triggering potential is similar in both young and old subduction zones. This is generally consistent with the observations that triggered tremor in the Nankai, Aleutian Arc, Alaska, and Vancouver Island was initiated by Love waves rather than the later passage of Rayleigh waves triggered by tremor bursts (e.g., Figs. 3, 5, 6, and 7).

For this simple modeling, the triggering potential for the Love and Rayleigh waves is calculated with a constant dominant period of 20 s and equal amplitude. In addition, as shown in Figure 9, tremor triggered by the Love and Rayleigh waves may occur in different regions, which would also result in different amplitudes. Finally, the comparisons

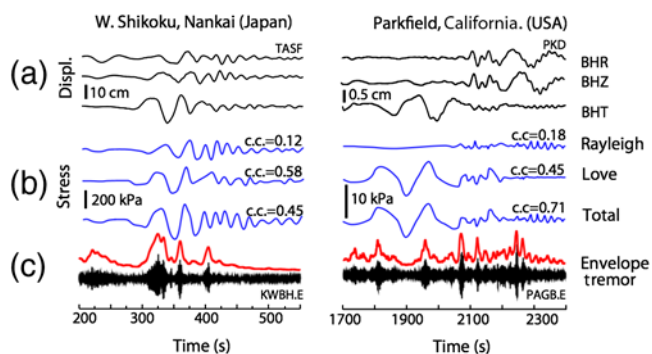


Figure 14. Time-dependent dynamic stress (stress grams) as a measurement of the surface-wave potential to trigger tremor in western Shikoku and Parkfield. (a) Radial, vertical, and transverse displacement components recorded by broadband seismic stations. (b) Dynamic stress caused by Love, Rayleigh, and combined (total) ground displacement. (c) Triggered tremor bursts shown in high-pass filtered and envelope-function seismograms. The cross correlation between dynamic stress grams and the envelope-function seismogram of triggered tremor is shown in (b). All signals have been time shifted back to the best-triggered tremor source. The color version of this figure is available only in the electronic edition.

between triggering potential and tremor amplitudes are qualitative. To obtain a more quantitative estimate of how dynamic stress triggers tremor, we need to know the precise amplitude and frequency of the triggering wave at the exact time when tremor pulse occurs, which can be accomplished by time shifting the triggered tremor and triggering waves back to the tremor source (e.g., Peng *et al.*, 2009; Rubinstein *et al.*, 2009). Therefore, precise triggered tremor locations and related fault-plane orientations are needed to produce an acceptable estimate of triggering dynamic stress.

In the second approach, we calculate the stress grams for two representative tectonic regions with precise triggered tremor locations: the Parkfield–Cholame strike-slip section of the SAF, and the subduction zone in Western Shikoku, Japan (Fig. 14). In both cases, we calculate individual dynamic stress tensors for surface waves with varying amplitudes and frequencies as measured from consecutive peaks in the displacement seismograms. Then, the time-dependent stress values are interpolated to obtain a continuous stress-gram signal. For the SAF, the stress grams are calculated for a vertical strike-slip right-lateral fault with a strike angle of 319° (Chao, Peng, Wu, *et al.*, 2012), and a tremor source of 25 km depth. For the western Shikoku, we use a tremor source of 35 km depth for a thrust fault of strike and dip angles of 225° and 15° , respectively (Miyazawa and Brodsky, 2008; Hill, 2010, 2012b; Table S4 in the electronic supplement). For both fault planes, we use a coefficient of static friction $\mu = 0.2$ (Hill, 2010, 2012b), as justified by the inference of near-lithostatic pore pressure at tremor depth from tidal correlations at Parkfield (Thomas *et al.*, 2009) and seismic tomography in other regions (Shelly *et al.*, 2006). We shift the tremor signals back to the source region based on a 1D velocity model in each region and use a constant phase velocity (4.1 km/s for the Love and 3.5 km/s for the

Rayleigh waves) to shift the time-dependent triggering potentials or dynamic stress grams back to the tremor source region (Miyazawa and Mori, 2006; Rubinstein *et al.*, 2007). We also take a smoothed-envelope function of the tremor signals and compute the cross correlations with the stress grams for the Love and Rayleigh waves and the sum traces separately.

In western Shikoku (Fig. 14a), the Love waves correlate better with the first two cycles of tremor bursts, but the later single tremor burst is not correlated well with either the Love or Rayleigh waves. At Parkfield (Fig. 14b), the first two cycles of tremor burst (between 1800 and 2000 s) are better correlated with the Love waves than they are later, when the tremor better associates with the Rayleigh waves. In both cases, the correlation coefficient values for the Love waves are higher than those for the Rayleigh waves, which is consistent with the higher triggering potential of Love waves (Fig. 13) and their larger amplitudes.

Discussion and Conclusion

In this study, we conducted a global search of deep tectonic tremor triggered by the 2011 M_w 9.0 Tohoku earthquake. Among the regions where either ambient or triggered tremor has been previously observed, we have found tremor triggered by the Tohoku mainshock in nine of these regions (Figs. 3–11). Such widespread triggering of tremor by the Tohoku mainshock is perhaps not surprising because the observed dynamic stress values at all of these regions equal or exceed 10 kPa (Fig. 2), which is close to or higher than the apparent triggering threshold found in previous studies (i.e., from 2 to 8 kPa) (Peng *et al.*, 2009; Rubinstein *et al.*, 2009; Chao, Peng, Wu, *et al.*, 2012). However, no clear evidence of tremor triggered by the Tohoku earthquake was found at either the CF in northern California or Guerrero, Mexico (Zigone *et al.*, 2012;  Figs. S3 and S4 in the electronic supplement). While we found several high-frequency signals recorded by a nearby broadband station in Nicoya Peninsula, Costa Rica, during the teleseismic surface waves ( Fig. S3 in the electronic supplement), we cannot verify the existence or lack of triggered tremor since additional waveform data are not yet open to the public. At the CF, while we did not identify coherent tremor-like signals in the band-pass-filtered seismograms ( Fig. S4 in the electronic supplement), we observed small-amplitude tremor signals in the surface broadband and borehole short-period recordings at the SJF in southern California (Fig. 10). We cannot rule out the possibility that weak tremor was triggered in the CF, but it was not detected because its amplitude is smaller than or close to that of background noise. Hence, we imply that tremor could be triggered in wider tectonic regions than we previously expected yet could remain undetected because its amplitude is below the noise level.

In places where ambient tremor was previously reported (e.g., southwest Japan, Taiwan, Aleutian Arc, Alaska, Cascadia, Parkfield, and New Zealand), triggered tremor was

generally observed near the ambient tremor sources. In southwest Japan, triggered tremor appeared to occur in the up-dip direction as compared with the location of most ambient tremor. Even if we perform a grid search at depths of 0–60 km, the horizontal locations in these regions vary only within $\pm 0.02^\circ$, suggesting that fixing tremor depth would not affect the horizontal location significantly. Although we could explain such observations as depth-dependent behavior of triggered and ambient tremor (e.g., Wech and Creager, 2011), triggered and ambient tremor in southwest Japan were located using different techniques. Hence, the apparent differences in the horizontal locations of triggered and ambient tremor could simply have originated from the use of varying location techniques rather than from genuine differences in behavior.

Parkfield is the only region where triggered and ambient tremor was identified and located with the same technique by Shelly and Hardebeck (2010). Shelly *et al.* (2011) summarized previous observations of triggered tremor in that region and found that the shallowest (< 20 km) tremor families in the creeping section of the SAF were infrequently triggered. However, it is not clear whether such a difference is caused by depth-dependent tremor behavior or variations in the tremor amplitudes, in which concurrent strong tremor sources mask weak tremor sources. We also examined the ratios between the number of tremor that occurred during the teleseismic surface waves to the total number of tremor that occurred within six days before the Tohoku mainshock (Fig. 9b). We found that only deep tremor (e.g., > 20 km) in the creeping section of the SAF was triggered, which is similar to the general patterns observed by Shelly *et al.* (2011). However, such a pattern is unclear for tremor sources near Cholame. Further systematic studies could verify any systematic differences between the locations of triggered and ambient tremor and identify the cause of possible depth-dependent tremor behaviors in the creeping section of the SAF. Nevertheless, it is evident that triggered and ambient tremor at Parkfield shares the same LFE template families.

This suggests that both types of tremor originated from the same source but that triggered tremor are driven by the extra stress changes from the surface waves (Shelly *et al.*, 2011). Because we are using waveforms of existing LFE families to detect within triggered tremor, only those LFE events with similar waveforms would be detected. However, the fact that we have detected 39 LFE events within 650 s of the teleseismic waves (with an average of 3.6 events per minute) suggests that these LFE families could explain most of the triggered tremor signals.

We found a positive correlation between the amplitudes of triggered tremor and the amplitudes of the associated dynamic stresses of the teleseismic surface waves in all regions (Fig. 12). This observation is consistent with the predictions of the clock-advance model (Gomberg, 2010) that larger triggering waves result in larger triggered tremor signals. For example, in the SJF, the PGV measured at station RDM during the Tohoku mainshock was ~ 0.12 cm/s, about one-fifth of the PGV of 0.54 cm/s during the 2002 Denali

fault earthquake (Chao, Peng, Fabian, *et al.*, 2012). The median triggered tremor amplitude was ~ 0.2 and ~ 10 nm/s for the Tohoku and Denali fault earthquake, respectively, which is again qualitatively consistent with the prediction of the clock-advance model. This finding also suggests that in regions where the background tremor rate is low (e.g., the SJF or the CF in California) or the background seismic noise is high, larger triggering waves are needed to trigger tremor with amplitudes above the background noise level. Although the correlation between the PGV and tremor amplitude is statistically significant, the data points are somewhat scattered, and the scatter becomes larger after the tremor amplitude corrections. The later is likely caused by the assumption of a constant Q , location errors, and/or other unknown path or site effects that modify the high-frequency tremor amplitudes. In addition, we also did not take into account differences among the background tremor rates in each region.

Finally, we systematically modeled the triggering potentials of Love and Rayleigh waves using a simple Coulomb failure criterion (Hill, 2010, 2012b). Our modeling results confirmed that both Love and Rayleigh waves play important roles in the triggering of tremor and that their triggering potentials are partially controlled by the incident angles of incoming surface waves (Fig. 13). We also computed the time-dependent stress changes for the Love and Rayleigh waves, or stress grams, and compared them with the tremor signals. We found that tremor pulses do not necessarily correlate with the peaks in any of the three displacement components but correlate better with the peaks in the calculated triggering potential, i.e., stress grams (Fig. 14). In other words, tremor-triggering potential could be caused by the combination of the dynamic stresses from both surface waves. This is particularly true following the arrival of a Rayleigh wave when Love- and Rayleigh-wave stresses may interfere constructively. This observation indicates that amplitudes and incidence angles of both Love and Rayleigh waves must be taken into account when evaluating their triggering potentials.

The fact that tremor amplitude is controlled mainly by the triggering waves and the background tremor rate, indicates that one could theoretically predict the occurrence of triggered tremor in certain regions immediately after the occurrence of major earthquakes and before the arrival of surface waves. The amplitudes of triggered tremor are ~ 10 – 100 nm/s, which is equivalent to a magnitude 0 to 1 earthquake. Hence, although triggered tremor does not cause any damage, it provides a useful tool to study how large earthquakes could change tremor behaviors and affect the deep fault zone behaviors at long-range distances.

Data and Resources

Seismograms used in this study were downloaded from the following resources: (1) Alaska and the Aleutian Arc: the Alaska Volcano Observatory (Network code: AV) distributed through the Incorporated Research Institutions for Seismology (IRIS) website (<http://www.iris.edu/mda>, last accessed

March 2012); (2) Vancouver Island, central Cascadia, and south Oregon, Cascadia subduction zone: the Canadian National Seismograph Network (http://www.earthquakescanada.nrcan.gc.ca/stndon/AutoDRM/autodrm_req-eng.php, last accessed March 2012) operated by the Geological Survey of Canada, and the Pacific Northwest Regional Seismic Network (Network code: UW), the Berkeley Digital Seismograph Network (Network code: BK), the Northern California Earthquake Data Center (Network codes PB), and the EarthScope (TA.L04D), distributed through the IRIS website (<http://www.iris.edu/mda>, last accessed November 2012); (3) the Nankai subduction zone, Japan: the Hi-net (High Sensitivity Seismograph Network, <http://www.hinet.bosai.go.jp/>, permission required, last accessed March 2012) and F-net (Broadband Seismograph Network, <http://www.fnet.bosai.go.jp/>, permission required, last accessed March 2012) operated by the National Research Institute for Earth Science and Disaster Prevention, Japan; (4) New Zealand: the New Zealand National Seismic Network (<http://www.geonet.org.nz/>, last accessed March 2012), operated by GNS Science; (5) others: the Calaveras fault (BK.MHC), Costa Rica (IL.JTS), and Cuba (CU.GTBY), all from the Berkeley Digital Seismograph Network (Network code: BK), and the Global Seismograph Network (Network code: II), the USGS Caribbean Network (Network code: CU), distributed through the IRIS website (<http://www.iris.edu/mda>, last accessed March 2012); (6) Parkfield: the Northern California Earthquake Data Center (network codes: BP, NC, and PB, <http://www.ncedc.org/>, last accessed March 2012); (7) the SJF: the Southern California Earthquake Data Center (network codes: AZ, CI and PB, <http://www.data.scec.org/>, last accessed March 2012); and (8) Taiwan: the Broadband Array in Taiwan for Seismology (<http://bats.earth.sinica.edu.tw/>, last accessed March 2012), operated by the Institute of Earth Sciences, Academia Sinica, and the short-period Central Weather Bureau Seismic Network (<http://gdms.cwb.gov.tw/>, permission required, last accessed March 2012), operated by the Taiwan Central Weather Bureau. The Waveform Envelope Correlation and Clustering (WECC) Cascadia tremor catalog was downloaded from <http://www.pnsn.org/tremor/>, last accessed December, 2012. Maps were generated by M_Map: a mapping package for Matlab (available at <http://www.eos.ubc.ca/~rich/map.html>, last accessed November, 2012).

Acknowledgments

The manuscript benefited from comments by Andy Newman, reviewers David Hill and Debi Kilb, and Guest Editor Justin Rubinstein. We thank David Shelly and Aaron Wech for allowing the use of their tremor catalogs at Parkfield and Cascadia, respectively. K. C., Z. P., and C. A. are supported by the National Science Foundation (NSF) through awards EAR-0908310 and EAR-0956051, and the Southern California Earthquake Center (SCEC). K. C. is also supported by the Japan Society for the Promotion of Science (JSPS) through awards P12329 and KAKENHI 23244091. C. A. is also supported by the NSF Graduate Fellowship Grant NSF Grant DGE-1148903. H.G.-H. and V.A.A. are supported by NSF Grant EAR-1053355. All maps in this paper were generated by the mapping toolbox developed by Rich Pawlowicz (see [Data and Resources](#)).

References

- Aiken, C., Z. Peng, and K. Chao (2013). Tremors along the Queen Charlotte Fault triggered by large teleseismic earthquakes, *Geophys. Res. Lett.* **40**, 1–6, doi: [10.1002/grl.50220](https://doi.org/10.1002/grl.50220).
- Aki, K., and P. G. Richards (2002). *Quantitative Seismology*, 2nd Ed., Univ. Sci. Books, Sausalito, California, 700 pp.
- Beroza, G. C., and S. Ide (2011). Slow earthquakes and nonvolcanic tremor, *Annu. Rev. Earth Planet. Sci.* **39**, 271–296, doi: [10.1146/annurev-earth-040809-152531](https://doi.org/10.1146/annurev-earth-040809-152531).
- Boore, D. M. (2003). Simulation of ground motion using the stochastic method, *Pure Appl. Geophys.* 635–676, doi: [10.1007/978-3-0348-8010-7_10](https://doi.org/10.1007/978-3-0348-8010-7_10).
- Brown, J. R., G. C. Beroza, S. Ide, K. Ohta, D. R. Shelly, S. Y. Schwartz, W. Rabbel, M. Thorwart, and H. Kao (2009). Deep low-frequency earthquakes in tremor localize to the plate interface in multiple subduction zones, *Geophys. Res. Lett.* **36**, L19306, doi: [10.1029/2009GL040027](https://doi.org/10.1029/2009GL040027).
- Brown, J. R., S. G. Prejean, G. C. Beroza, J. S. Gombert, and P. J. Haeussler (2013). Deep low-frequency earthquakes in Tectonic tremor along the Alaska–Aleutian subduction zone, *J. Geophys. Res.* **118**, doi: [10.1029/2012JB009459](https://doi.org/10.1029/2012JB009459).
- Chao, K., Z. Peng, A. Fabian, and L. Ojha (2012). Comparisons of triggered tremor in California, *Bull. Seismol. Soc. Am.* **12**, no. 2, 900–908, doi: [10.1785/0120110151](https://doi.org/10.1785/0120110151).
- Chao, K., Z. Peng, A. Wech, C.-C. Tang, C.-H. Lin, and C.-H. Chen (2011). Deep tremor activities beneath the Central Range in Taiwan and their relationship to local, regional, and teleseismic earthquakes, *Seismol. Res. Lett.* **82**, 326.
- Chao, K., Z. Peng, C. Wu, C.-C. Tang, and C.-H. Lin (2012). Remote triggering of non-volcanic tremor around Taiwan, *Geophys. J. Int.* **188**, no. 1, 301–324, doi: [10.1111/j.1365-246X.2011.05261.x](https://doi.org/10.1111/j.1365-246X.2011.05261.x).
- Delahaye, E., J. Townend, M. Reyners, and G. Rogers (2009). Microseismicity but no tremor accompanying slow slip in the Hikurangi subduction zone, New Zealand, *Earth Planet. Sci. Lett.* **277**, 1–2, 21–28, doi: [10.1016/j.epsl.2008.09.038](https://doi.org/10.1016/j.epsl.2008.09.038).
- Enescu, B., K. Chao, Z. Peng, H. Gonzalez-Huizar, K. Obara, D. P. Hill, T. Matsuzawa, S. Tanaka, K. Shiomi, T. Takeda, and A. A. Velasco (2012). Love wave triggering of non-volcanic tremor in the Nankai region, southwest Japan: Observations and physical interpretation (abstract S33B-2550), *AGU (Fall Meet.) San Francisco, California*, 3–7 December, S33B-2550.
- Flinchum, B. A., and M. R. Brudzinski (2011). Non-volcanic tremor triggered by teleseismic surface waves in south-central Alaska, *Eos Trans. AGU, Fall Meet. Suppl.*, Abstract S23B-2254.
- Fry, B., K. Chao, S. Bannister, and Z. Peng (2011). Deep tremor in New Zealand triggered by the 2010 M_w 8.8 Chile earthquake, *Geophys. Res. Lett.* **38**, L15306, doi: [10.1029/2011GL048319](https://doi.org/10.1029/2011GL048319).
- Geller, R. J. (1976). Scaling relations for earthquake source parameters and magnitudes, *Bull. Seismol. Soc. Am.* **66**, no. 5, 1501–1523.
- Gombert, J. (2010). Lessons from (triggered) tremor, *J. Geophys. Res.* **115**, B10302, doi: [10.1029/2009JB007011](https://doi.org/10.1029/2009JB007011).
- Gombert, J., and the Cascadia 2007 and Beyond Working Group (2010). Slow-slip phenomena in Cascadia from 2007 and beyond: A review, *GSA Bull.* **122**, no. 7/8, 963–978, doi: [10.1130/B30287.1](https://doi.org/10.1130/B30287.1).
- Gombert, J., J. L. Rubinstein, and Z. Peng (2008). Widespread triggering of nonvolcanic tremor in California, *Science* **319**, 173, doi: [10.1126/science.1149164](https://doi.org/10.1126/science.1149164).
- Gonzalez-Huizar, H., and A. A. Velasco (2011). Dynamic triggering: Stress modeling and a case study, *J. Geophys. Res.* **116**, B02304, doi: [10.1029/2009JB007000](https://doi.org/10.1029/2009JB007000).
- Gonzalez-Huizar, H., A. A. Velasco, Z. Peng, and R. Castro (2012). Remote triggered seismicity caused by the 2011, M 9.0 Tohoku, Japan earthquake, *Geophys. Res. Lett.* L10302, doi: [10.1029/2012GL051015](https://doi.org/10.1029/2012GL051015).
- Guilhem, A., Z. Peng, and R. M. Nadeau (2010). High-frequency identification of non-volcanic tremor triggered by regional earthquakes, *Geophys. Res. Lett.* **37**, L16309, doi: [10.1029/2010GL044660](https://doi.org/10.1029/2010GL044660).
- Hill, D. (2008). Dynamic stresses, Coulomb failure, and remote triggering, *Bull. Seismol. Soc. Am.* **98**, no. 1, 66–92, doi: [10.1785/0120070049](https://doi.org/10.1785/0120070049).
- Hill, D. P. (2010). Surface-wave potential for triggering tectonic (nonvolcanic) tremor, *Bull. Seismol. Soc. Am.* **100**, no. 5A, 1859–1878, doi: [10.1785/0120090362](https://doi.org/10.1785/0120090362).
- Hill, D. P. (2012a). Dynamic stress, Coulomb failure, and remote triggering—Corrected, *Bull. Seismol. Soc. Am.* **102**, no. 6, 2313–2336.
- Hill, D. P. (2012b). Surface-wave potential for triggering tectonic (nonvolcanic) tremor—Corrected, *Bull. Seismol. Soc. Am.* **102**, no. 6, 2337–2355.
- Hill, D. P., Z. Peng, D. R. Shelly, and C. Aiken (2013). S-wave triggering of tremor beneath the Parkfield, California, section of the San Andreas fault by the 2011 Tohoku, Japan, earthquake: Observations and theory, *Bull. Seismol. Soc. Am.* **103**, no. 2B, doi: [10.1785/0120120114](https://doi.org/10.1785/0120120114).
- Hillers, G., and J. P. Ampuero (2009). Systematic search for spontaneous non-volcanic tremor in Southern California, *Eos Trans. AGU* **90**, no. 54, Fall Meet. Suppl., Abstract T13D-1918.
- Ide, S. (2010). Striations, duration, migration and tidal response in deep tremor, *Nature* **466**, 356–359, doi: [10.1038/nature09251](https://doi.org/10.1038/nature09251).
- Ide, S. (2012). Variety and spatial heterogeneity of tectonic tremor worldwide, *J. Geophys. Res.* **117**, no. B3, doi: [10.1029/2011JB008840](https://doi.org/10.1029/2011JB008840).
- Kao, H., and S.-J. Shan (2004). The Source-Scanning Algorithm: Mapping the distribution of seismic sources in time and space, *Geophys. J. Int.* **157**, no. 2, 589–594, doi: [10.1111/j.1365-246X.2004.02276.x](https://doi.org/10.1111/j.1365-246X.2004.02276.x).
- Kao, H., K. Wang, H. Dragert, J. Y. Kao, and G. Rogers (2010). Estimating seismic moment magnitude (M_w) of tremor bursts in northern Cascadia: Implications for the “seismic efficiency” of episodic tremor and slip, *Geophys. Res. Lett.* **37**, no. 19, doi: [10.1029/2010GL044927](https://doi.org/10.1029/2010GL044927).
- Kim, M. J., S. Y. Schwartz, and S. Bannister (2011). Non-volcanic tremor associated with the March 2010 Gisborne slow slip event at the Hikurangi subduction margin, New Zealand, *Geophys. Res. Lett.* **38**, no. 14, doi: [10.1029/2011GL048400](https://doi.org/10.1029/2011GL048400).
- Kostoglodov, V., A. Husker, N. M. Shapiro, J. S. Payero, M. Campillo, N. Cotte, and R. Clayton (2010). The 2006 slow slip event and non-volcanic tremor in the Mexican subduction zone, *Geophys. Res. Lett.* **37**, 24301, doi: [10.1029/2010GL045424](https://doi.org/10.1029/2010GL045424).
- Lay, T., and T. C. Wallace (1995). *Modern Global Seismology*, Academic, San Diego, California, 381–383.
- McCaffrey, R., L. M. Wallace, and J. Beavan (2008). Slow slip and frictional transition at low temperature at the Hikurangi subduction zone, *Nature Geosci.* **1**, no. 5, 316–320, doi: [10.1038/geo178](https://doi.org/10.1038/geo178).
- Miller, M. M., T. Melbourne, D. J. Johnson, and W. Q. Sumner (2002). Periodic slow earthquakes from the Cascadia subduction zone, *Science* **295**, 2423, doi: [10.1126/science.1071193](https://doi.org/10.1126/science.1071193).
- Miyazawa, M. (2011). Propagation of an earthquake triggering front from the 2011 Tohoku-Oki earthquake, *Geophys. Res. Lett.* **38**, no. 23, doi: [10.1029/2011GL049795](https://doi.org/10.1029/2011GL049795).
- Miyazawa, M., and E. Brodsky (2008). Deep low-frequency tremor that correlates with passing surface waves, *J. Geophys. Res.* **113**, B01307, doi: [10.1029/2006JB004890](https://doi.org/10.1029/2006JB004890).
- Miyazawa, M., and J. Mori (2005). Detection of triggered deep low-frequency events from the 2003 Tokachi-oki earthquake, *Geophys. Res. Lett.* **32**, L10307, doi: [10.1029/2005GL022539](https://doi.org/10.1029/2005GL022539).
- Miyazawa, M., and J. Mori (2006). Evidence suggesting fluid flow beneath Japan due to periodic seismic triggering from the 2004 Sumatra-Andaman earthquake, *Geophys. Res. Lett.* **33**, L05303, doi: [10.1029/2005GL025087](https://doi.org/10.1029/2005GL025087).
- Miyazawa, M., E. Brodsky, and J. Mori (2008). Learning from dynamic triggering of low-frequency tremor in subduction zones, *Earth Planets Space* **60**, e17–e20.
- Nadeau, R. M., and D. Dolenc (2005). Nonvolcanic tremors deep beneath the San Andreas fault, *Science* **307**, no. 389, doi: [10.1126/science.1107142](https://doi.org/10.1126/science.1107142).
- Nadeau, R. M., and A. Guilhem (2009). Nonvolcanic tremor evolution and the San Simeon and Parkfield, California, earthquakes, *Science* **325**, 191–193, doi: [10.1126/science.1174155](https://doi.org/10.1126/science.1174155).
- Obara, K. (2002). Nonvolcanic deep tremor associated with subduction in southwest Japan, *Science* **296**, 1679–1681, doi: [10.1126/science.1070378](https://doi.org/10.1126/science.1070378).

- Obara, K. (2011). Characteristics and interactions between non-volcanic tremor and related slow earthquakes in the Nankai subduction zone, southwest Japan, *J. Geodyn.* **52**, no. 3–4, 229–248, doi: [10.1016/j.jog.2011.04.002](https://doi.org/10.1016/j.jog.2011.04.002).
- Obara, K., S. Tanaka, T. Maeda, and T. Matsuzawa (2010). Depth-dependent activity of non-volcanic tremor in southwest Japan, *Geophys. Res. Lett.* **37**, no. 13, doi: [10.1029/2010GL043679](https://doi.org/10.1029/2010GL043679).
- Outerbridge, K. C., T. H. Dixon, S. Y. Schwartz, J. I. Walter, M. Protti, V. Gonzalez, J. Biggs, M. M. Thorwart, and W. Rabbel (2010). A tremor and slip event on the Cocos-Caribbean subduction zone as measured by a global positioning system (GPS) and seismic network on the Nicoya Peninsula, Costa Rica, *J. Geophys. Res.* **115**, B10408, doi: [10.1029/2009JB006845](https://doi.org/10.1029/2009JB006845).
- Payero, J. S., V. Kostoglodov, N. Shapiro, T. Mikumo, A. Iglesias, X. Perez-Campos, and R. W. Clayton (2008). Nonvolcanic tremor observed in the Mexican subduction zone, *Geophys. Res. Lett.* **35**, L07305, doi: [10.1029/2007GL032877](https://doi.org/10.1029/2007GL032877).
- Peng, Z., and K. Chao (2008). Non-volcanic tremor beneath the Central Range in Taiwan triggered by the 2001 M_w 7.8 Kunlun earthquake, *Geophys. J. Int.* **175**, no. 2, 825–829, doi: [10.1111/j.1365-246X.2008.03886.x](https://doi.org/10.1111/j.1365-246X.2008.03886.x).
- Peng, Z., and J. Gomberg (2010). An integrated perspective of the continuum between earthquakes and slow-slip phenomena, *Nature Geosci.* **3**, 599–607, doi: [10.1038/ngeo940](https://doi.org/10.1038/ngeo940).
- Peng, Z., K. Chao, C. Wu, B. Fry, B. Enescu, and C. Aiken (2012). Global observations of triggered tectonic tremor, *Seismol. Res. Lett.* **83**, no. 2, 417.
- Peng, Z., H. Gonzalez-Huizar, K. Chao, C. Aiken, B. Moreno, and G. Armstrong (2013). Tectonic tremor beneath Cuba triggered by the M_w 8.8 Maule and M_w 9.0 Tohoku-Oki earthquakes, *Bull. Seismol. Soc. Am.* **103**, no. 1, 595–600, doi: [10.1785/0120120253](https://doi.org/10.1785/0120120253).
- Peng, Z., D. P. Hill, D. R. Shelly, and C. Aiken (2010). Remotely triggered microearthquakes and tremor in central California following the 2010 M_w 8.8 Chile Earthquake, *Geophys. Res. Lett.* **37**, L24312, doi: [10.1029/2010GL045462](https://doi.org/10.1029/2010GL045462).
- Peng, Z., L. T. Long, and P. Zhao (2011). The relevance of high-frequency analysis artifacts to remote triggering, *Seismol. Res. Lett.* **82**, no. 5, 654–660, doi: [10.1785/gssrl.82.5.654](https://doi.org/10.1785/gssrl.82.5.654).
- Peng, Z., J. E. Vidale, K. C. Creager, J. L. Rubinstein, J. Gomberg, and P. Bodin (2008). Strong tremor near Parkfield, CA, excited by the 2002 Denali Fault earthquake, *Geophys. Res. Lett.* **35**, L23305, doi: [10.1029/2008GL036080](https://doi.org/10.1029/2008GL036080).
- Peng, Z., J. E. Vidale, A. G. Wech, R. M. Nadeau, and K. C. Creager (2009). Remote triggering of tremor along the San Andreas fault in central California, *J. Geophys. Res.* **114**, B00A06, doi: [10.1029/2008JB006049](https://doi.org/10.1029/2008JB006049).
- Peterson, C., and D. Christensen (2009). Possible relationship between nonvolcanic tremor and the 1998–2001 slow slip event, south central Alaska, *J. Geophys. Res.* **114**, B06302, doi: [10.1029/2008JB006096](https://doi.org/10.1029/2008JB006096).
- Peterson, C., S. McNutt, and D. Christensen (2011). Nonvolcanic tremor in the Aleutian Arc, *Bull. Seismol. Soc. Am.* **101**, no. 6, 3081–3087, doi: [10.1785/0120100241](https://doi.org/10.1785/0120100241).
- Rogers, G., and H. Dragert (2003). Episodic tremor and slip on the Cascadia subduction zone: The chatter of silent slip, *Science* **300**, 1942–1943, doi: [10.1126/science.1084783](https://doi.org/10.1126/science.1084783).
- Rubinstein, J. L., G. C. Beroza, J. Brown, M. Brudzinski, K. Chao, J. Gomberg, S. Malone, D. Oppenheimer, Z. Peng, S. Prejean, H. Savage, D. R. Shelly, A. Wech, and M. West (2011). Widespread triggering of earthquakes and tremor by the 2011 off-Tohoku earthquake, *Seismol. Res. Lett.* **82**, 461.
- Rubinstein, J. L., J. Gomberg, J. E. Vidale, A. G. Wech, H. Kao, K. C. Creager, and G. Rogers (2009). Seismic wave triggering of nonvolcanic tremor, episodic tremor and slip, and earthquakes on Vancouver Island, *J. Geophys. Res.* **114**, B00A01, doi: [10.1029/2008JB005875](https://doi.org/10.1029/2008JB005875).
- Rubinstein, J. L., J. E. Vidale, J. Gomberg, P. Bodin, K. C. Creager, and S. D. Malone (2007). Non-volcanic tremor driven by large transient shear stresses, *Nature* **448**, 579–582, doi: [10.1038/nature06017](https://doi.org/10.1038/nature06017).
- Shearer, P. M. (1999). *Introduction to Seismology*, Cambridge University Press, Cambridge, United Kingdom, 163–165.
- Shelly, D. R., and J. L. Hardebeck (2010). Precise tremor source locations and amplitude variations along the lower-crustal central San Andreas fault, *Geophys. Res. Lett.* **37**, L14301, doi: [10.1029/2010GL043672](https://doi.org/10.1029/2010GL043672).
- Shelly, D. R., G. C. Beroza, and S. Ide (2007). Non-volcanic tremor and low-frequency earthquake swarms, *Nature* **446**, no. 7133, 305–307, doi: [10.1038/nature05666](https://doi.org/10.1038/nature05666).
- Shelly, D. R., G. C. Beroza, S. Ide, and S. Nakamura (2006). Low-frequency earthquakes in Shikoku, Japan, and their relationship to episodic tremor and slip, *Nature* **442**, no. 7099, 188–191, doi: [10.1038/nature04931](https://doi.org/10.1038/nature04931).
- Shelly, D. R., W. L. Ellsworth, T. Ryberg, C. Haberland, G. S. Fuis, J. Murphy, R. M. Nadeau, and R. Bürgmann (2009). Precise location of San Andreas fault tremors near Cholame, California using seismometer clusters: Slip on the deep extension of the fault? *Geophys. Res. Lett.* **36**, L01303, doi: [10.1029/2008GL036367](https://doi.org/10.1029/2008GL036367).
- Shelly, D. R., Z. Peng, D. P. Hill, and C. Aiken (2011). Triggered creep as a possible mechanism for delayed dynamic triggering of tremor and earthquakes, *Nature Geosci.* **4**, 384–388, doi: [10.1038/ngeo1141](https://doi.org/10.1038/ngeo1141).
- Stein, S., and M. Wysession (2003). *An Introduction to Seismology, Earthquakes and Earth Structure*, Blackwell Publishing, 263–266.
- Swiecki, Z., and S. Y. Schwartz (2010). Ambient tremor, but no triggered tremor at the northern Costa Rica subduction zone, *Eos Trans. AGU*, Fall Meet. Suppl., Abstract S23A-2108.
- Tang, C.-C., Z. Peng, K. Chao, C.-H. Chen, and C.-H. Lin (2010). Detecting low-frequency earthquakes within non-volcanic tremor in southern Taiwan triggered by the 2005 M_w 8.6 Nias earthquake, *Geophys. Res. Lett.* **37**, L16307, doi: [10.1029/2010GL043918](https://doi.org/10.1029/2010GL043918).
- Thomas, A. M., R. M. Nadeau, and R. Bürgmann (2009). Tremor-tide correlations and near-lithostatic pore pressure on the deep San Andreas fault, *Nature* **462**, no. 7276, 1048–1051, doi: [10.1038/nature08654](https://doi.org/10.1038/nature08654).
- van der Elst, N. J., and E. E. Brodsky (2010). Connecting near-field and far-field earthquake triggering to dynamic strain, *J. Geophys. Res.* **115**, no. B7, doi: [10.1029/2009JB006681](https://doi.org/10.1029/2009JB006681).
- Wallace, L. M., and J. Beavan (2010). Diverse slow slip behavior at the Hikurangi subduction margin, New Zealand, *J. Geophys. Res.* **115**, no. B12, doi: [10.1029/2010JB007717](https://doi.org/10.1029/2010JB007717).
- Wallace, L. M., J. Beavan, R. McCaffrey, and D. Darby (2004). Subduction zone coupling and tectonic block rotations in the North Island, New Zealand, *J. Geophys. Res.* **109**, no. B12, doi: [10.1029/2004JB003241](https://doi.org/10.1029/2004JB003241).
- Walter, J. I., S. Y. Schwartz, J. M. Protti, and V. Gonzalez (2011). Persistent tremor within the northern Costa Rica seismogenic zone, *Geophys. Res. Lett.* **38**, L01307, doi: [10.1029/2010GL045586](https://doi.org/10.1029/2010GL045586).
- Wang, W., X. Gong, Z. Peng, Q. Chen, and C. Wu (2011). Dynamic triggering around Fangshan Pluton near Beijing, China, *Eos Trans. AGU*, Fall Meet. Suppl., Abstract S22B-06.
- Wech, A. G. (2010). Interactive tremor monitoring, *Seismol. Res. Lett.* **81**, no. 4, 664–669, doi: [10.1785/gssrl.81.4.664](https://doi.org/10.1785/gssrl.81.4.664).
- Wech, A. G., and K. C. Creager (2008). Automated detection and location of Cascadia tremor, *Geophys. Res. Lett.* **35**, 20, doi: [10.1029/2008GL035458](https://doi.org/10.1029/2008GL035458).
- Wech, A. G., and K. C. Creager (2011). A continuum of stress, strength and slip in the Cascadia subduction zone, *Nature Geosci.* **4**, no. 9, 624–628, doi: [10.1038/ngeo1215](https://doi.org/10.1038/ngeo1215).
- Wech, A. G., C. M. Boese, T. A. Stern, and J. Townend (2012). Tectonic tremor and deep slow slip on the Alpine fault, *Geophys. Res. Lett.* **39**, 10, doi: [10.1029/2012GL051751](https://doi.org/10.1029/2012GL051751).
- Zigone, D., D. Rivet, M. Radiguet, M. Campillo, C. Voisin, N. Cotte, A. Walpersdorf, N. M. Shapiro, G. Cougoulat, P. Roux, V. Kostoglodov, A. Husker, and J. S. Payero (2012). Triggering of tremors and slow slip event in Guerrero, Mexico, by the 2010 M_w 8.8 Maule, Chile, earthquake, *J. Geophys. Res.* **117**, B09304, doi: [10.1029/2012JB009160](https://doi.org/10.1029/2012JB009160).

Appendix A

The tremor location is calculated by performing a grid search of the minimal root mean square (rms) between the

theoretical and observed travel-time differences ($\Delta T_{i,j}$) for all station pairs (pair ^{i,j}) (Peng and Chao, 2008; Peng *et al.*, 2009; Chao, Peng, Wu, *et al.*, 2012). Because tremor is primarily generated by shear failure at depth, we qualitatively explore horizontal seismograms, and for those that show clear tremor bursts, we compute the envelope function of the seismograms. If N stations are used to locate tremor, the total number of station pairs is $n^{i,j} = N(N - 1)/2$. The equation for computing the rms for each grid point ($[x, y, z]$ or [longitude, latitude, depth]) is

$$\begin{aligned} \text{rms}_{(x,y,z)} &= \sqrt{\sum_{i=1,j=2}^n (\Delta T_{i,j})^2/n} = \sqrt{\left(\sum_{i=1,j=2}^n (\Delta t_{i,j}^{\text{theo}} - \Delta t_{i,j}^{\text{obs}})^2/n\right)} \\ &= \sqrt{\frac{(\Delta t_{1,2}^{\text{theo}} - \Delta t_{1,2}^{\text{obs}})^2 + (\Delta t_{1,3}^{\text{theo}} - \Delta t_{1,3}^{\text{obs}})^2 + \dots + (\Delta t_{2,3}^{\text{theo}} - \Delta t_{2,3}^{\text{obs}})^2 + \dots + (\Delta t_{i=n-1,j=n}^{\text{theo}} - \Delta t_{i=n-1,j=n}^{\text{obs}})^2}{n}}, \quad (\text{A1}) \end{aligned}$$

where theo and obs denote the theoretical and observed travel-time differences ($\Delta T_{i,j}$), respectively, for all pairs (\sum pair ^{i,j}). For each single pair ^{i,j} , the theoretical travel-time difference ($\Delta t_{i,j}^{\text{theo}}$) is computed from the difference of S -wave travel times from a common source (x, y, z) to different stations i and j based on a 1D velocity model in each region (Ⓔ Table S3 in the electronic supplement). The observed travel-time difference ($\Delta t_{i,j}^{\text{obs}}$) is computed from a cross correlation of envelope functions for each tremor burst.

The best tremor location (x, y, z)^{best} for each tremor burst corresponds to the minimum rms within the entire grid search space. The final tremor location for each triggering event is calculated by averaging the locations from different tremor bursts weighted by the rms.

Because the tremor depth is generally not well constrained, in this study, we fix the tremor depth to a fixed value in each region (Ⓔ Table S1 in the electronic supplement). Hence, the grid search is performed in the longitude and latitude in only a grid space of 0.01° .

For regions with multiple tremor sources, we first qualitatively separate the observed tremor signals into several groups based on their different waveform characteristics and moveout. This is done as follows. First, the seismograms observed at all stations that recorded clear tremor bursts are plotted along the strike of the plate interface. If the tremor originates from different sources, we would expect to see a different moveout pattern for different individual bursts.

Next, we try to locate initial sources of individual tremor bursts and use the moveout plot (i.e., seismograms plotted relative to the distance between the recording station and the tremor source) to confirm whether or not the location is reliable. We use different combinations of nearby stations until we obtain stable tremor sources. We consider multiple tremor sources if their epicenters are at least 30 km distance apart, which is larger than the location errors of each tremor source. For tremor sources within 30 km, an average, stable location is obtained from individual tremor bursts.

School of Earth and Atmospheric Sciences
Georgia Institute of Technology
311 Ferst Drive
Atlanta, Georgia 30332
(K.C., Z.P., C.A.)

Geological Sciences
University of Texas at El Paso
500 W. University Ave.
El Paso, Texas 79902
(H.G., A.A.V.)

National Research Institute for Earth Science and Disaster Prevention
(NIED)
3-1 Tennodai, Tsukuba
Ibaraki 305-0006, Japan
(B.E., T.M.)

Geological Survey of Canada
Pacific Geoscience Centre
9860 West Saanich Road
Sidney, BC V8L 4B2, Canada
(H.K.)

Earthquake Research Institute
University of Tokyo
1-1-1 Yayoi, Bunkyo-ku
Tokyo 113-0032, Japan
(K.O.)